Evolution of the Palaeotethys in the Eastern Mediterranean: A multi-method approach to unravel the age, provenance and tectonic setting of the Upper Palaeozoic Konya Complex and its Mesozoic cover sequence (south-central Turkey)

Kersten Löwen[a], Guido Meinhold[a, b], Arzu Arslan[c], Talip Güngör[d] and Jasper Berndt[e]

[a]Abteilung Sedimentologie/Umweltgeologie, Geowissenschaftliches Zentrum Göttingen, Universität Göttingen, Goldschmidtstraße 3, 37077 Göttingen, Germany;

[b]School of Geography, Geology and the Environment, Keele University, ST5 5BG, UK;

[c]Newcastle-under-Lyme, Staffordshire, ST5 2ND, UK;

[d]Department of Geological Engineering, Dokuz Eylül University, Tınaztepe Campus, 35160 Buca-İzmir, Turkey;

[e]Institute of Mineralogy, Westfälische Wilhelms-University Münster, Corrensstraße 24, 48149 Münster, Germany

Guido Meinhold, https://orcid.org/0000-0001-8375-8375

Arzu Arslan, https://orcid.org/0000-0002-1556-9166

CONTACT: Kersten Löwen; kersten.loewen@geo.uni-goettingen.de; Abteilung Sedimentologie/Umweltgeologie, Geowissenschaftliches Zentrum Göttingen, Universität Göttingen, Goldschmidtstraße 3, 37077 Göttingen, Germany

Abstract

Thirteen siliciclastic sediments from the Upper Palaeozoic Konya Complex and its Mesozoic cover were studied by a multi-method approach combining thin-section petrography, bulk-rock geochemistry, mineral chemistry of rutile, and U–Pb geochronology of detrital zircons. Provenance sensitive data of samples from the Upper Palaeozoic Halıcı Formation indicate sediment supply from mainly low- to medium-grade metamorphosed sedimentary rocks of felsic character, while the contribution from volcanic rocks was rare. The detrital zircon record of sediments from the Halıcı Formation documents sediment supply from different sources and excludes a similar provenance. Some samples show great similarities with Palaeozoic sandstones from the cover sequence of the Saharan Metacraton and the Arabian–Nubian Shield, while the other samples indicate a provenance that must be sought in units with a southern Eurasian affinity. The upper limit for sediment deposition in the Halıcı Formation is mostly constrained by Early Palaeozoic zircon populations; however, sediment accumulation in Pennsylvanian–Cisuralian time is more likely, contemporaneously with the Upper Palaeozoic succession on the Karaburun Peninsula (western Turkey). The provenance of sediments from the Upper Triassic Ardıçlı Formation remains enigmatic, but the source should be sought nonetheless in units close to the depositional site. In any case, detrital zircon age spectra and compositional data exclude recycling of underlying rock units (i.e. Halıcı Formation). Overall, our new provenance data reveal great similarities between the Konya Complex and comparable units (Chios, Karaburun) but also highlight distinct differences in terms of sediment composition and provenance.

Keywords: Palaeotethys; Turkey; Konya Complex; Sediment provenance; U-Pb geochronology; Whole-rock geochemistry; Rutile geochemistry

Supplemental data for this article can be accessed xxxxxx.

1. Introduction

The Eastern Mediterranean region experienced intense geodynamic reorganization during the Palaeozoic and Mesozoic era due to the opening and closure of the Palaeo- and Neotethyan oceans (e.g. Şengör and Yılmaz 1981; Şengör *et al.* 1984; Okay and Tüysüz 1999; Stampfli and Borel 2002). As a result, the geology of Turkey was shaped by the accretion of several oceanic and continental fragments (Figure 1a).

The study area, located ca. 30 km NW of Konya city in south-central Turkey, is part of the Afyon Zone on the northern margin of the Anatolide–Tauride Block (Figure 1a). The Anatolide–Tauride Block is subdivided into an unmetamorphosed Gondwana-derived southern part referred to as Taurides and the northerly Anatolides representing the northern margin of the Palaeotethys in Palaeozoic time. Northward subduction of the Palaeotethys during the Carboniferous led to the formation of magmatic arc/fore-arc complexes and to the amalgamation of both blocks in latest Triassic time when the Palaeotethys (supposedly) finally closed (e.g. Stampfli *et al.* 2001a, 2001b; Stampfli and Borel 2002; Moix *et al.* 2008). In an alternative view, the Anatolide–Tauride Block is interpreted as part of the passive northern margin of Gondwana that switched to an active margin with induced back-arc rifting during the Carboniferous (e.g. Göncüoğlu *et al.* 2007; Robertson and Ustaömer 2009a, 2009b). Some of the models that advocate southward subduction beneath the northern margin of Gondwana do not necessarily exclude northward subduction beneath Eurasia (Robertson and Ustaömer 2009a).

Different palaeotectonic models and implications for the evolution of the Palaeotethys are strongly debated in the literature. In this regard, the investigation of Palaeozoic and Mesozoic ocean-related sedimentary successions is of special importance. Such occurrences are sparse in the Eastern Mediterranean since they are either overlain by younger Mesozoic units or primary structures and information are obscured by metamorphism and/or deformation due to Alpine overprint. However, Upper Palaeozoic and Lower Mesozoic Palaeotethys-related successions have been identified on the Aegean island of Chios (Greece), the Karaburun Peninsula (western Turkey) and in our study area, the Konya

Complex (name adopted from Robertson and Ustaömer 2009b) in south-central Turkey. Even though these areas have been the subject of several studies their role within the Palaeotethyan realm is controversial. Provenance data have been published for the islands of Chios and Inousses (Meinhold *et al.* 2007, 2008a, b; Meinhold and Frei 2008) and recently for the Karaburun Peninsula (Löwen *et al.* 2017, 2018). This kind of data is crucial for the understanding of the evolution of the Palaeotethys but is not yet available for the Konya Complex.

In our study, we present results from thin-section petrography, whole-rock geochemistry, single-grain geochemistry of detrital rutile and U–Pb dating of detrital zircons from Upper Palaeozoic–Lower Mesozoic sediments from the Konya Complex. The new data provide insight into their age, composition and provenance and contribute to a better understanding of the origin of the sedimentary successions and the closure history of the Palaeotethys.

2. Geological setting

The Konya Complex comprises a complex mixture of Upper Silurian to Upper Cretaceous rocks including a Palaeozoic carbonate platform, an Upper Palaeozoic mélange unit and Permian–Triassic cover units. Basic palaeontological studies have provided a good biostratigraphic framework (Eren 1993b; Kurt 1994; Göncüoğlu *et al.* 2000) and other studies addressed the nature of the metasedimentary matrix and embedded blocks of the Palaeozoic mélange (e.g. Eren *et al.* 2004; Robertson and Ustaömer 2009b, 2011). During the last decades, several geological maps of the area have been presented and alternative tectonostratigraphic schemes using nonuniform nomenclature of formations were discussed in the literature (Figure 2). The main dissension centres around the question whether the Konya Complex is largely interpreted as a mélange (Robertson and Ustaömer 2009b), existed as a single overall stratigraphic succession (Özcan *et al.* 1988, 1990) or is subdivided into a lower autochthon and upper allochthon related to Alpine deformation (Eren 1993b; Eren *et al.* 2004). For a better understanding, a stratigraphic panel illustrating the various stratigraphic schemes and nomenclature used by different authors is provided (Figure 2).

The oldest rocks in the study area belong to the Bozdağ Formation that mainly crops out NW of Ardıçlı village. It is interpreted as a massive, reefal carbonate platform containing abundant micro- and macrofossils (e.g. fusulinids, crinoids, corals, and trilobites) of Late Silurian–Early Devonian (Göncüoğlu *et al.* 2000), Middle–Late Devonian and Early Carboniferous age (Eren 1993b; Kurt 1994). It passes upwards into a mélange unit that comprises a variety of rock types and is widely exposed in the central and NW part of the study area (Figure 1b). The mélange is largely equivalent to the Bağrıkurt Formation of the Sızma Group described by Eren *et al.* (2004) and the Halıcı Formation of Özcan *et al.* (1988, 1990), respectively. It comprises an (often) strongly folded and foliated metasedimentary matrix made up of alternations of phyllites, mudstones, (turbiditic) sandstones, quartzites, conglomerates, limestones and black chert with exotic blocks/olistoliths. The main types are carbonates (limestones and dolomites) – mostly derived from the underlying Bozdağ Formation – black chert and minor basic igneous rocks.

Corals and fusulinids from limestone blocks yielded Late Silurian–Devonian and Early Carboniferous ages and blocks of black chert have been dated as Late Silurian–Early Devonian using microfossils and conodonts (Özcan *et al.* 1990; Eren 1993b; Göncüoğlu and Kozur 1998; Kozur 1999; Eren and Kurt 2000; Göncüoğlu *et al.* 2000, 2007). The depositional age of the siliciclastic matrix is only poorly constrained. Locally, Early Carboniferous (Visean) fossils from limestones that either represent detached blocks within the matrix or belong to the matrix itself have been reported by Özcan *et al.* (1990) and Göncüoğlu *et al.* (2007). Even a Permian age was discussed based on fossils from metacarbonate intercalations indicative of that period (Eren 1996). Furthermore, meta-igneous rocks of basaltic to rhyolitic composition (Özcan *et al.* 1990) are widely exposed in an area SW of Bağrıkurt village and N to NE of Sızma town (Figure 1b) and are referred to as Kadınhanı metamagmatics by Eren *et al.* (2004). The age of these rocks is only poorly constrained to Early Permian by preliminary radiometric data (Candan *et al.* 2009), but an Early Triassic age has also been reported for trachyandesitic metavolcanics (Akal *et al.* 2012). The stratigraphic position and relationship to the adjacent sedimentary rocks have not

yet been completely clarified. They were interpreted as dikes and sills crosscutting the Bozdağ Formation and alternatively, as lava flows or blocks within the siliciclastic rocks of the Halıcı Formation (Özcan *et al.* 1990; Eren 2001; Eren *et al.* 2004). However, contact relations are often obscure and the existence of a separate, mappable volcano-sedimentary unit including the Kadınhanı metamagmatics and siliciclastic sequences was proposed by Robertson and Ustaömer (2009b).

The Halıcı Formation is unconformably overlain by the Eldeş Formation which comprises a thick sedimentary succession and mainly crops out in the western part of the study area, south of Eldeş (Figure 1b). It corresponds to the Lower (Derbent Formation) and Middle (Aladağ Formation) unit of the Gökçeyurt Group described by Eren (1993a) and Eren *et al.* (2004) and was interpreted as (para)autochthonous and structurally lowermost sequence. On the contrary, according to Robertson and Ustaömer (2009b), these sediments unconformably overlay the mélange unit although the original contact was not observed due to the presence of a Cenozoic sedimentary cover. The Eldeş Formation is dominantly composed of alternations of dark grey fossiliferous limestones, marbles, phyllites, and quartzites containing a rich faunal assemblage of Late Permian age (Eren 1993b). Separated by an angular unconformity, these rocks are overlain by a transgressive sequence of violet coloured siliciclastic sediments of the Ardıçlı Formation interfingering with metacarbonates that contain Early Triassic foraminifera and conodonts (Özcan *et al.* 1988, 1990). It is conformably covered by thick, Upper Triassic–Jurassic limestone and dolomite of the Loras Formation and Jurassic–Cretaceous cherty limestone and mudstone of the Midos Tepe Formation (also known as Midos Formation), which are equivalent to the Upper unit of the Gökçeyurt Group autochthon (Göğer and Kıral 1969; Özcan *et al.* 1990; Eren 1993b). These carbonates are tectonically overlain by Neotethyan-related magmatic and metamorphic units that are exposed in an area SW of Konya city (Figure 1b). They comprise the Hatip ophiolitic mélange including harzburgite blocks (locally with high-grade metamorphic sole rocks) and the Çayırbağ ophiolite of Late Cretaceous age. Recently obtained $^{40}Ar/^{39}Ar$ data from amphibolites of the metamorphic sole yielded ages ranging from 87.04 ± 0.36 to 84.66 ± 0.30

166 Ma and were interpreted to date the timing of metamorphism (Daşçı *et al.* 2015). Overall, the
167 autochthonous and allochthonous rocks in the study area were overprinted by multi-phase
168 Alpine deformation (e.g. Eren 2001; Eren *et al.* 2004; Robertson and Ustaömer 2009b).
169
170 **3. Methods**
171 Thirteen sandstone samples were collected from outcrops NW of Konya town, ten from the
172 Upper Palaeozoic Halıcı Formation and three from the Lower Mesozoic Ardıçlı Formation
173 and were prepared for petrographic, bulk-rock geochemical and single-grain chemical (rutile)
174 and geochronological (zircon) analyses (Table S1). These formations were targeted as they
175 show great similarities in terms of lithology and age with comparable successions on Chios
176 Island and the Karaburun Peninsula further to the west (Figure 1b). The Chios–Karaburun
177 units have recently been studied in detail and provenance data have become available.
178 Thin sections were prepared from all samples and were analysed using a petrographic
179 microscope. Mineralogical composition was determined by point-counting of at least 300
180 grains of mono- and polycrystalline quartz (Q_m, Q_p), plagioclase feldspar (P), alkali feldspar
181 (Kfs) and lithic fragments (L_v, L_s) following the Gazzi-Dickinson method. Matrix and cement
182 were not counted but estimated using standard comparison charts for visual estimation.
183 Whole-rock geochemical major and trace element analyses were conducted using a
184 PANalytical AXIOS Advanced sequential X-ray spectrometer. Fused glass discs were
185 produced by adding Spectromelt® and LiF to the sample powder and melting in platinum
186 crucibles. Loss on ignition (LOI) was determined gravimetrically by stepwise heating to
187 1000 °C.
188 Solution inductively coupled plasma mass spectrometry (ICP–MS) was applied for rare earth
189 element geochemistry. The analysis was performed on a ThermoElectron VG PlasmaQuad 2
190 quadrupole ICP–MS.
191 Zircon and rutile grains for mineral chemical and geochronological analyses were randomly
192 selected by handpicking from the 63–250 μm fraction. Mineral grains were mounted in epoxy
193 discs composed of Araldite® and hardener (mixed 5:1) and polished to expose the grain

interior. Prior to U–Pb zircon dating, cathodoluminescence (CL) imaging was applied to reveal internal structures and to guide spot placement. The age determination was carried out on a sector-field ICP–MS (Element2, ThermoFisher) coupled to a 193-nm Analyte G2 Excimer Laser Ablation System at the Institute of Mineralogy of the University Münster.

Prior to geochemical analysis of rutile the polished grain mounts were carbon-coated to ensure conductivity. Measurements were carried out with a JEOL JXA 8900 RL electron microprobe analyzer (EMPA) equipped with five wavelength dispersive spectrometers.

Detailed descriptions of sample preparation, analytical techniques and the compiled analytical data are available in the online Supplementary Material.

4. Results

Here we present a compilation of new petrographic (Figure 4), radiometric and geochemical data from sedimentary sequences of the Konya area. Emphasis was placed on the Upper Palaeozoic Halıcı Formation that is widely exposed in the central and eastern part of the study area (Figure 1b) and the Lower Triassic Ardıçlı Formation from the Mesozoic cover sequence.

4.1 Field Observations

We divide the Halıcı Formation into two subunits based on our field observations. Part of the formation is characterized by alternations of low-grade phyllitic rocks (Figure 3a) with intercalations of limestones, fine- to medium-grained sandstones, conglomerates and cherts and includes isolated blocks/olistoliths of different lithologies (e.g. cherts, limestones, igneous rocks). In the following, we are referring to it as a mélange unit, which represents the actual mélange as described above. Although we consider the mélange unit as a single and differentiable complex, we recognize that it could be made up of several subunits. The phyllitic rocks of the mélange unit often contain large Fe-oxide pseudomorphs after pyrite, indicative of anoxic, probably deep-water conditions. Additionally, we are introducing the term ‘flysch’ unit to describe a low-grade metamorphosed part of the Halıcı Formation that is

free of any blocks/olistoliths and was deposited on top of the mélange unit. It mainly comprises mudstones, siltstones, well-bedded sandstones (Figure 3b, c), locally also containing plant fossils and Fe-oxide pseudomorphs. We prefer using inverted commas for the term ‘flysch’ as we use it as a descriptive lithofacies term, following Sestini (1970, p. 562) and Mitchell and Reading (1986, p. 477).

Even though the Konya Complex has been studied for decades, its internal tectonostratigraphy is not yet fully understood since the study area experienced Alpine deformation and large-scale folding and contacts are often covered by younger sediments. In this respect, the valley extending over a distance of ca. 10 km from the villages of Ardıçlı to Yükselen Bilecik (in NW direction) has turned out to be one of the key areas for illustrating its complex internal structure (Figure 1b). Close to Ardıçlı, a thick succession of Palaeozoic sediments and the Mesozoic cover sequence are well exposed on the slopes of the valley over several tens to hundreds of meters. From bottom to top the sequence starts with limestone of the Bozdağ Formation (Figure 2d). This limestone is in parts conglomeratic and contains pebbles and slightly deformed corals (Figure 3d). The Bozdağ Formation is unconformably overlain by the mélange unit, but in some areas, the mélange unit is likely missing and the ‘flysch’ unit is unconformably above the Bozdağ Formation (Figure 2d). The supposed unconformable contact between the ‘flysch’ unit and Bozdağ limestone is exposed in an old quarry, located ca. 4 km to the west of Ardıçlı. At this place, the massive limestones are conformably covered by sedimentary rocks of the ‘flysch’ unit (Figure 3e). These include conglomerates with phyllitic pebbles, probably from a reworked material of the mélange unit, which is situated in deeper levels. The contact between these rocks and the Bozdağ limestone can be observed elsewhere in the study area and is (probably) of tectonic nature. In these cases, the sediments are intensely folded and deformed close to the contact with the Bozdağ Formation (Figure 3f). From the Permian–Triassic cover units, the Eldeş Formation of Eren (1993b) is not present in the study area around Ardıçlı. However, the Triassic Ardıçlı Formation is present and consists of a characteristic purple-coloured siliciclastic material with carbonate intercalations (Figure 3g). The succession ends with a

thick sequence of massive, well-bedded Mesozoic limestones of the Loras Formation at the top (Figure 3h).

4.2 Sediment petrography

Important parameters that were considered during petrographic analysis to describe sediment properties are given in Table S2. These include results from point counting for QFL classification, observed accessory minerals and textural information (grain-size, sorting, roundness). For classification of sandstones we used the scheme proposed by Dott (1964) to account for variable proportions of matrix material in our samples.

The analysis has shown that samples from the Halıcı Formation have high percentages of quartz (average 87%) and only contain low amounts of feldspars (≤14%) and lithic fragments (≤12%) (Figure 4). Rocks from the mélange unit are classified as subarkoses (Figure 5a, 6a, d) and lithic/arkosic wackes (Figure 5c–d, 6b–c, e) with a low textural maturity and highly variable matrix contents of 5–50%. Some samples show evidence for strong chemical alteration (Figure 5a) and also foliation and shearing (Figure 6b, d). The above-mentioned sandstones represent the sedimentary matrix, the exception being a lithic wacke (T14-34) (Figure 5d, 6e) that was identified as a larger block/olistolith (several meters) embedded in the siliciclastic rocks. Samples from the 'flysch' unit comprise one pair of subarkose and quartzarenite rocks and one pair of more immature lithic/arkosic wackes (Figure 4, Table S2). The former are highly mature (Q: 91–98%) and contain a very low amount of matrix material (<5%), negligible amounts of lithic fragments and rare feldspars (Figure 5b). In contrast, the latter are characterized by higher amounts feldspars (8–14%) and lithic fragments (6–12%) in a fine-grained matrix (Figure 5e, 6f–g). The most common accessory phases in these samples are tourmaline, rutile, zircon, titanite and Fe-oxides. The majority of lithic fragments (>90%) was derived from (meta)sediments (quartzites, mica-schists and rare chert), whereas volcanic fragments are rare and were primarily observed in wackes of the 'flysch' unit (Figure 6a–g). Observed petrographic features of these sandstones are in good agreement with

277 previous descriptions of the Halıcı Formation (e.g. Kurt 1997; Robertson and Ustaömer
278 2011).
279 Studied sediments from the Ardıçlı Formation are of different composition and texture (Figure
280 5f–h). One quartzitic litharenite (T14-29) is characterized by a fine-grained quartzitic matrix
281 with poorly sorted, large (up to 1400 µm) grains of mono- and polycrystalline quartz and rare
282 sedimentary fragments (Figure 5g). Textural features are shear bands that are associated
283 with muscovite and abundant fine particles of Fe-oxides. In contrast, sample T14-30 is a
284 metaconglomerate composed of a mica-dominated matrix with deformed large (up to 1.4 cm)
285 sedimentary and volcanic fragments (chert, quartzite, schists, felsic plutonic rocks) (Figures
286 5f, 6h).
287
288 ***4.3 Whole-rock geochemistry***
289 Major and trace element compositions of samples from the Konya Complex are shown in
290 Figures 7, 8, 9. Siliciclastic rocks from the mélange unit of the Halıcı Formation have
291 moderate to high SiO_2 (70–88 wt.%) and moderate Al_2O_3 (7–14 wt.%) concentrations and low
292 Na_2O (0.4–3.2 wt.%) contents. The concentration of K_2O is generally low (1.4–2.8 wt.%), but
293 the highest measured concentration is at almost 5%, caused by high amounts of
294 phyllosilicates as indicated by high Rb contents. Sandstones from the 'flysch' unit are
295 characterized by on average slightly higher SiO_2 (76–90 wt.%) but lower Al_2O_3 (5–11 wt.%),
296 K_2O (<2 wt.%) and Na_2O (<2 wt.%) concentrations. Two samples from the Ardıçlı Formation
297 are very similar in their major element composition with high SiO_2 (90–95 wt.%) and very low
298 K_2O (≤1.1 wt.%) concentrations and a lack of Na_2O. In contrast, the conglomeratic sample
299 (T14–30) from this formation has highest Al_2O_3 (16.5%) and K_2O (4.4%) and Rb (192 ppm)
300 due to the dominance of mica in its fine-grained matrix.
301 Selected trace elements for samples of the Konya area and data of Upper Palaeozoic and
302 Triassic sandstones from the Karaburun Peninsula in western Turkey (Löwen *et al.* 2018)
303 have been normalized to the upper continental crust (UCC) and are shown in multi-element
304 diagrams (Figure 8a–c). Most trace elements are slight to moderately depleted compared to

UCC for all but one sample from the Ardıçlı Formation (T14-30) and exhibit pronounced negative anomalies for Sr, Y, Cr and Ni. Heaviest depletion in both, trace elements and rare earth elements (REE) is revealed by a highly mature quartz arenite (T14-23) from the 'flysch' unit due to dilution effects from high quartz contents. Chondrite-normalized REE patterns of the studied sediments and UCC and Post-Archaean Australian Average Shale (PAAS) reference values are shown in Figure 8d–f. In general, the REE geochemistry of most samples is characterized by lower total REE concentrations compared to UCC and PAAS, a (heavy) fractionation between light rare earth elements (LREE) and heavy rare earth elements (HREE) and a slightly negative Eu anomaly (calculated from $Eu/Eu^* = Eu_N/(Sm_N \times Gd_N)^{0.5}$ = 0.47–0.87), with the exception of sample T14-34 (Eu/Eu* = 1.07). The average total amount of REE concentrations is lower in the 'flysch' unit (∑REE = 80.77 ppm) compared to the mélange unit (∑REE = 124.61 ppm). Highest total REE concentrations (∑REE = 373.61 ppm) and very strong fractionation of LREE and HREE (La_N/Yb_N = 39.97) can be observed in the Ardıçlı Formation (T14-30). The degree of fractionation is highly variable in the mélange unit (La_N/Yb_N = 5.74–30.24) and is lower in the 'flysch' unit (La_N/Yb_N = 4.84–10.18).

The different behaviour (e.g. mobility, compatibility) of specific trace elements in sediments allows using their concentrations and/or elemental ratios as proxies to identify input from either felsic or (ultra)mafic sources. In a compilation of discrimination diagrams utilizing these characteristics, the signature of our samples suggests the supply of detritus from predominantly felsic source rocks (Figure 9). However, one sample from the Ardıçlı Formation (T14-30) is characterized by high Ni and Cr concentrations as well as high Cr/V (2.65) and low Y/Ni (0.15) ratios, which is indicative for the presence of (ultra)mafic components. In contrast, rocks from the 'flysch' unit have generally low concentrations of Cr (13–170 ppm) and Ni (6–37 ppm) that are even lower in samples from the mélange unit (4–58 and 1–34 ppm, respectively) (Figure 9b). Slight indication for (ultra)mafic detritus in these samples is given by relatively high Cr, Cr/V and Cr/Th values in combination with low Y/Ni and Th/Sc ratios as observed in an arkosic wacke from the 'flysch' unit (T14-36) (Figure 9b–d).

333

334 ***4.4 Detrital zircon geochronology***

335 *4.4.1 Halıcı Formation - mélange unit*

336 Detrital zircons from sample T14-20B are of comparatively small size (<100 μm) and have a
337 pinkish colour. The grains are generally well rounded and often show oscillatory zoning
338 patterns. U–Pb ages were obtained from 99 grains of which 73 were accepted (based on the
339 criteria outlined in the methods section in the Supplementary Material). The data define a
340 polymodal age spectrum from 423 Ma to 2.6 Ga with a gap of ages from 1.2 to 1.8 Ga
341 (Figure 10a). Almost 25% of the zircons are of a Palaeozoic age with a major Cambrian–
342 Ordovician population, but the dominant group (49%) occurs in the Neoproterozoic. The
343 youngest coherent age group (n = 3) occurs at ~450–460 Ma and the youngest single grain
344 yielded an age of 423.4 ± 13.5 Ma.

345 Zircon grains from sample T14-31 are colourless to pinkish and often well rounded (>50%)
346 while euhedral grains are rare. CL imaging revealed mainly oscillatory and rare sector zoning
347 as well as some thin metamorphic overgrowths. The dataset includes 100 spots of which 89
348 yielded concordant ages. The total spectrum of filtered ages ranges from 478 Ma to 3.0 Ga,
349 comprising a minor number of zircons from 1.2 to 1.9 Ga (Figure 10c). A large Proterozoic
350 population (87%) with a dominating Neoproterozoic age group exists and Palaeozoic grains
351 are virtually absent. The youngest single spot ages are 478 ± 11 Ma and 495 ± 7 Ma, but the
352 youngest group (n = 4) of coherent U–Pb ages occurs at ~530–545 Ma.

353 The analysed grains of sample T14-34 often have elongated, euhedral shapes and are
354 characterized by a comparatively dark pinkish colour and show either oscillatory or banded
355 CL patterns (Figure S2 in Supplementary Material). In total, 99 spots were analysed and
356 filtered data contain 94 U–Pb ages, ranging from 413 Ma to 2.0 Ga (Figure 10e). Most of the
357 grains (~85%) are of Palaeozoic age and define a unimodal, Ordovician–Silurian population.
358 The youngest group of coherent zircon ages (n = 21) occurs at ~440–450 Ma but two
359 younger, post-Silurian grains exist as well.

360

361 *4.4.2 Halıcı Formation – 'flysch' unit*

362 The majority of zircon grains from sample T14-22 are light pinkish in colour and well-rounded
363 or subhedral. Oscillatory zoning is a common feature, and some grains show thin
364 metamorphic overgrowths. U–Pb ages were obtained from 94 spots and filtered data (*n* = 84)
365 show an age spectrum from 407 Ma to 2.7 Ga (Figure 10b). Palaeozoic zircons are present
366 in small amounts only, and the bulk population is dominated by a large number of
367 Proterozoic – mainly Neoproterozoic (59%) – grains while zircons with ages of 1.2–1.9 Ga
368 are lacking. The youngest single grains yielded ages of 407.8 ± 13.8 and 420.5 ± 13.7 Ma,
369 but a group (*n* = 5) of coherent U–Pb ages occurs at ~430–440 Ma.

370 The dataset of sample T14-36 comprises 100 spots with 94 accepted U–Pb ages. The grains
371 are mostly rounded or subhedral, have a pinkish or occasionally darker colour and often
372 reveal oscillatory zoning. The age spectrum ranges from 326 Ma to 3.1 Ga and is dominated
373 by a Palaeozoic (primarily Devonian) population (64%) and an additional Neoproterozoic age
374 group (10%) (Figure 10d). Two single spot ages occur at 326.3 ± 5.3 and 328.3 ± 328.3 Ma
375 followed by a group (*n* = 14) of coherent grains at ~360–380 Ma.

376 For sample T14-39, data were obtained from 100 single grains that yielded 89 concordant U–
377 Pb ages. The majority of zircons are pinkish in colour, have rounded or subhedral shapes
378 and reveal oscillatory zoning or homogeneous CL patterns. The data show a polymodal age
379 distribution ranging from 305 Ma to 3.3 Ga with a dominant Palaeozoic (43%), mainly
380 Carboniferous–Devonian and minor Neoproterozoic population (Figure 10f). The youngest
381 group (*n* = 8) of zircons occurs at ~340–350 Ma but three Late Carboniferous single spot
382 ages define the lower limit of the spectrum.

383

384 *4.4.3 Ardıçlı Formation*

385 Detrital zircons from sample T14-29 are pinkish in colour and characterized by a high amount
386 of subhedral to euhedral grains, almost exclusively with oscillatory zoning. A total of 100
387 grains were analysed and yielded 99 concordant U–Pb ages. The spectrum shows a
388 unimodal age distribution with dominant Triassic (64%) and Permian (20%) populations and

389 isolated single grains with a maximum age of 1.4 Ga (Figure 10g). Two single grains at 165
390 and 175 Ma define the lower limit of the spectrum while the youngest coherent group (*n* = 5)
391 occurs at ~220 Ma. It is worth mentioning that the youngest eight grains are characterized by
392 high (>1000 ppm, up to 3600 ppm) U concentrations.
393 Zircons separated from sample T14-30 comprise the biggest population of euhedral grains
394 (35%), are comparatively large (>150 µm) and reveal a characteristic dark pinkish to
395 brownish colour. A total of 102 spots were analysed and filtered data (*n* = 91) show unimodal
396 age spectra with a well-defined Triassic population (84%) (Figure 10h). The age spectrum
397 ranges from 138 Ma to 900 Ma but only three grains are of pre-Mesozoic age. A special
398 feature of most grains is their very low CL luminescence and notably high U concentrations
399 of up to 3600 ppm (~2274 ppm average).
400
401 *4.5 Rutile geochemistry*
402 Rutile is mainly formed in medium- to high-grade metamorphic rocks (i.e. eclogites,
403 granulites, high-grade metasediments), which are considered as the primary source for
404 detrital rutile (e.g. Meinhold 2010, and references therein). Its high chemical and physical
405 resistance and widespread appearance in sedimentary rocks make rutile a valuable mineral
406 for provenance studies. Information on source rock lithology can be inferred from trace
407 element composition, in particular the Cr–Nb system. For discrimination of rutiles from
408 metamafic and metafelsic sources, the most recent criterion proposed by Triebold *et al.*
409 (2012) was used:
410 $$x = 5 \times (Nb_{ppm} - 500) - Cr_{ppm}$$
411
412 where metamafic rutiles have negative values and metafelsic rutiles have positive values .
413 Grains with Nb and Cr concentration below the detection limit were not considered for
414 calculation.
415 Additionally, it has been demonstrated that Zr incorporation in rutile is strongly temperature
416 dependent in quartz and zircon-bearing systems (e.g. Zack *et al.* 2004; Tomkins *et al.* 2007).

417 In this study, formation temperatures of rutile were calculated using the thermometer
418 equation of Tomkins *et al.* (2007):

419 $$T(°C) = \frac{83.9 + 0.410 \times P}{0.1428 - R \times \ln Zr_{ppm}} - 273$$

420

421 with the gas constant R (0.0083144 kJ/K) and P = 10 kbar (default setting, as no pressure
422 information is available for the detrital rutile grains).
423 For source rock classification and temperature calculations, a total of 178 single rutile grains
424 from six sandstone samples of the Halıcı and Ardıçlı formations were analysed by EMPA.
425 Results for source rock classification and calculated formation temperatures are shown in
426 Figure 11. The data are indicative of prevailing metafelsic sources for all but one sample.
427 Results from both samples of the mélange unit are congruent and suggest that ca. 75% of
428 rutile grains were derived from metafelsic lithologies. In contrast, sandstones from the 'flysch'
429 unit contain rutiles with more variable Cr–Nb compositions. Results for a mature subarkose
430 (T14-22) clearly indicate supply of rutile from almost exclusively felsic source rocks (94%),
431 but the influence of mafic sources is increasing and even dominating (59%) in the arkosic
432 wackes (Figure 11a). Calculated formation temperatures for rutiles from the studied samples
433 range from 500°C to 850°C with a major population in the range of amphibolite- to eclogite-
434 facies conditions (Figure 11b). Temperatures from grains of the mélange unit are mainly
435 between 550°C and 650 °C (T14-20B) and 600–700°C (T14-31), respectively. Sandstones of
436 the 'flysch' unit seem to contain a higher proportion of rutiles formed under slightly lower
437 temperature conditions (550–600°C). It should be mentioned that calculation of formation
438 temperatures was not possible for a large number (70%) of rutile grains from sample T14-22
439 due to very low Zr concentrations (below detection limit). Results for the Ardıçlı Formation
440 also indicate a dominant metafelsic source for detrital rutiles. Calculated formation
441 temperatures range from 500°C to 850°C with a dominant population between 550°C and
442 700 °C.
443

444 **5. Discussion**

445 The palaeogeographic affinity (i.e. Eurasia- or Gondwana-related) and geodynamic evolution
446 of the Konya Complex and comparable units in western Turkey and the Aegean Sea (i.e.
447 Chios and Karaburun units) (Figure 1a) in Late Palaeozoic–Early Mesozoic times is strongly
448 debated in the scientific community. In this study, the terms 'Eurasia-related' or 'Eurasian
449 affinity' refer to terranes, which were once located along the periphery of Gondwana but
450 rifted off during the early Palaeozoic and were accreted to Eurasia at different times. The
451 terms 'Gondwana-related' or 'Gondwanan affinity' refer to units that were part of Gondwana
452 throughout most of the Palaeozoic.
453 The new petrographical, geochemical and chronological data from the Upper Palaeozoic
454 Halıcı Formation and its Mesozoic cover sequence are used here to determine their
455 maximum depositional ages and constrain their provenance. These parameters are
456 important prerequisites for understanding the depositional history of the Konya basin and to
457 test current tectonic and palaeogeographic reconstructions. To this day several alternative
458 interpretations have been proposed: (i) A Eurasian setting is inferred by Eren *et al.* (2004) in
459 which the Bozdağ limestone is interpreted as deposit at the northern passive margin of the
460 Palaeotethys. Early Carboniferous northward subduction induced the formation of a
461 magmatic arc and fore-arc basin and olistostrome deposition. (ii) An earlier model suggests
462 the formation of the Konya Complex along the northern passive margin of Gondwana.
463 Incipient southward subduction in Carboniferous times led to the construction of a continental
464 arc, which supplied detritus for the olistostromal unit (Eren and Kurt 2000). (iii) In contrast,
465 Özcan *et al.* (1988, 1990) interpreted the Konya Complex as a failed back-arc rift at the
466 northern margin of Gondwana related to southward subduction. The Palaeozoic Bozdağ
467 limestone rifted and subsided in Carboniferous time while olistostrome deposition occurred in
468 an intracontinental basin. (iv) Another alternative includes pre-Silurian rifting of a continental
469 fragment including the future Upper Palaeozoic carbonate platform away from the Gondwana
470 margin. Incipient southward subduction in mid-Carboniferous time led to re-accretion to the
471 continent and formation of the mélange (Robertson and Ustaömer 2009b). This model also
472 includes northward subduction beneath Eurasia accompanied by arc magmatism (e.g.

473 Sakarya arc). To sum up, the basic dissent in the discussion is related to the palaeoposition
474 of the Konya Complex during the Late Palaeozoic and the nature of the northern Gondwana
475 margin.
476
477 ***5.1 Maximum depositional ages***
478 Previous workers have already provided good age constraints from biostratigraphic data,
479 especially for the fossiliferous Bozdağ limestone and parts of the Permian–Cretaceous cover
480 units of the Konya area (Özcan *et al.* 1988, 1990; Eren 1993b; Eren *et al.* 2004; Kozur 1999;
481 Göncüoğlu *et al.* 2000). Biostratigraphic information is sparse in the Halıcı Formation, and
482 until now, radiometric data from detrital zircons of metasedimentary matrix rocks have not
483 been available. Data from limestone intercalations indicate an Early Carboniferous age
484 (Özcan *et al.* 1990) but also Early Permian fossils (fusulinids, corals, trilobites, crinoids) were
485 reported from the upper part of the Formation (Eren 1996). First U–Pb detrital zircon data
486 obtained from six sandstones of the Halıcı Formation presented in this study give insight into
487 the depositional history of these sediments. In the case of the block-bearing mélange unit,
488 the youngest zircon populations occur at ~450–460 Ma (T14-20B) and ~530–545 Ma (T14-
489 31). Slightly younger grains (~400–440 Ma) were identified in a lithic wacke (T14-34) that
490 represents a block in the mélange. Since sediment accumulation must have occurred
491 contemporaneously or after the emplacement of the youngest, Mississippian to
492 Serpukhovian–Bashkirian limestone blocks within the mélange (Göncüoğlu *et al.* 2007), the
493 actual depositional age of the matrix has to be younger than indicated by detrital zircons. In
494 contrast to the mélange unit, considerably younger Mississippian-aged zircons occur in two
495 arkosic wackes of the ‘flysch’ unit (Figure 10d, f), even though the youngest grains in a third
496 sample are of Silurian–Devonian age (Figure 10b). Given the age of the blocks, the youngest
497 detrital zircon populations in the sediments and reported biostratigraphic data we assume a
498 Pennsylvanian–Cisuralian depositional age for matrix rocks of the Halıcı Formation.
499 An Early Triassic age was assigned to the Ardıçlı Formation based on foraminifera and
500 conodonts described from metacarbonates interfingering with the siliciclastic sediments

(Özcan *et al.* 1988). However, Eren *et al.* (2004) assigned a ?Late Permian–Triassic age to this formation solely based on stratigraphic correlation, i.e. their Ertuğrul and Bahçecik formations which they further correlated to part of the autochthonous Gökçeyurt Group. Detrital zircons from two samples revealed considerably younger Jurassic and even Cretaceous ages. In any case, these results should be treated with caution due to the fact that especially the youngest grains are suffering from high (>1000 ppm) U concentrations and/or short signal intervals. We consider these ages as not reliable and rejected them for further interpretations (Figure 10g). The youngest group within the remaining population yielded Late Triassic (Norian) ages and is slightly younger than the previously inferred age. The issue of significantly U-rich grains that are affected by radiation damage (i.e. metamictization) is even more evident for zircons from sample T14-30. For this reason, the filtering criteria were tightened for this sample and only grains showing a difference of the U–Pb ages in the range of 5% and low (<1%) common Pb were considered. The residual population indicates a slightly younger latest Triassic–earliest Jurassic depositional age (Figure 10h).

5.2 Provenance

5.2.1 Upper Palaeozoic sediments

In terms of provenance the obtained age spectra exclude a common palaeogeographic origin for the Upper Palaeozoic sediments of the Halıcı Formation. The analysed samples reveal three different types of age spectra that rather suggest derivation of detritus from different source areas.

A first distinct group comprises two subarkoses from the mélange unit (T14-20B and T14-31) and a single one from the ‘flysch’ unit (T14-22). It is characterized by a variable (6–25%) Early Palaeozoic (mainly Cambrian–Ordovician) population, a high proportion (48–59%) of Neoproterozoic grains and a significant Tonian–Stenian age group (27–37%) (Figure 10a–c). Similar age spectra have lately been reported from Carboniferous sandstones of the Aladağ Nappe (eastern Taurides) and the Konya mélange (Ustaömer *et al.* 2016a, 2018) and were

attributed to source regions on the northern Gondwana continent. The lack of Devonian and post-Devonian grains indicates a source region isolated from Variscan influence. The Neoproterozoic population is dominated by Cryogenian–Ediacaran zircons, which can be related to several orogenic cycles in conjunction with the assembly of northern Gondwana (Cadomian–Pan-African orogeny), whereas the abundant Tonian–Stenian grains are attributed to Grenvillian orogenic events. The latter are rather sparse in siliciclastic rocks of western North Africa (Avigad *et al.* 2012), but have been recorded in sediments from central North Gondwana and the Afro-Arabian margin (i.e. Saharan Metacraton and Arabian–Nubian Shield) (Avigad *et al.* 2003; Kolodner *et al.* 2006; Be'eri-Shlevin *et al.* 2009; Meinhold *et al.* 2011). Apart from the additional Early Palaeozoic population, our samples show great similarities with Early to Middle Ordovician sandstones in southern Jordan (Kolodner *et al.* 2006) and Middle to Late Ordovician sandstones from the Murzuq and Kufra basins in Libya (Meinhold *et al.* 2011, 2013). In the Taurides, comparable signatures were observed in Cambrian–Triassic metasedimentary cover rocks of the Karacahisar dome in south-central Turkey. They were used to establish a close link between the Tauride Block and the Afro-Arabian margin, from Cambrian to at least Triassic time (Abbo *et al.* 2015). Further studies carried out Late Palaeozoic–Early Mesozoic sediments on Crete (Zulauf *et al.* 2016), Kythera (Marsellos *et al.* 2012) and the Peloponnesus (Chatzaras *et al.* 2016) also revealed zircon populations suggesting a northern Gondwana provenance. In contrast, cover rocks of the lower Tyros Unit on eastern Crete dominantly contain Variscan detritus and indicate deposition along the southern active margin of Eurasia (Zulauf *et al.* 2015, Chatzaras *et al.* 2016).

Furthermore, rutile chemistry and thermometry revealed the importance of amphibolite- to eclogite-facies rocks of predominantly acidic character in the source area. A small proportion (≤12%) of rutiles derived from high-T rocks has also been observed which requires the presence of a high-grade metamorphic source. Such rocks are rare in the Arabian–Nubian Shield and small occurrences of granulites and granulite-facies orthogneisses are only locally exposed in the Afif Terrane of Saudi Arabia and the Barka Terrane in Sudan, respectively

(Johnson and Woldehaimanot 2003). A more proximal source is represented by late Neoproterozoic granulites from the Pan-African basement in the Menderes Massif (Candan *et al.* 2001, and references therein).

A completely different age spectrum comprising a largely unimodal late Cambrian–Ordovician zircon population is obtained from a lithic wacke (T14-34) of the mélange unit (Figure 10e). Igneous source rocks of corresponding age are well known from the larger study area and have been ascribed to rifting processes related to the opening of the Rheic Ocean along the northern margin of Gondwana (von Raumer *et al.* 2002). Cambrian U–Pb zircon ages of 511 ± 16 Ma and 514 ± 14 Ma are documented from the pre-Alpine basement of eastern Crete (Romano *et al.* 2004). Evidence for Middle to Late Ordovician magmatism is present from metagranite occurrences in the Tavşanlı Zone (467 ± 5 Ma, Okay *et al.* 2008; 446 ± 8 Ma, Özbey *et al.* 2013) of the Anatolide–Tauride Block. They are interpreted to represent regional rifting events at the northern Gondwana margin. Other examples of Early and Middle Ordovician magmatism are documented from basement rocks of the Biga Peninsula of the Sakarya Zone (462 ± 6 Ma, Özmen and Reischmann 1999), gneisses of the Sredna Gora Zone (480 ± 30 Ma, 485 ± 50 Ma, Peytcheva and von Quadt 2004) and granites of the Serbo-Macedonian Massif (460 ± 8 Ma, Titorenkova *et al.* 2003) in the Balkan region. In contrast, Ordovician magmatic activity has not been reported from terranes of the Arabian plate. Considering the low textural maturity of the sediment and high proportion of euhedral and angular zircon grains, a proximal provenance is likely. Furthermore, the abundance of volcanic quartz grains and lack of rutile suggest a significant contribution from igneous rocks in the source region. Thus, we assume the lithic wacke (T14-34) was originally deposited at northern margin of Gondwana, in proximity to Cambrian–Ordovician felsic igneous rocks related to the opening of the Rheic Ocean.

A third group of detrital zircon spectra has been detected in two lithic/arkosic wackes from the ‘flysch’ unit (T14-36 and T14-39). They contain dominantly Devonian–Carboniferous (34–57%), small Neoproterozoic (10–33 %) but only minor Tonian–Stenian populations (1–10 %) (Figure 10d, f). With respect to provenance, a large number of Devonian-aged grains is of

585 special importance as it allows narrowing down possible source areas that are restricted to
586 very few localities only. The closest known exposures of igneous bodies are the Çamlık
587 granodiorite (398 ± 1 Ma, Okay *et al.* 1996, 2006) and the Karacabey Pluton (394 ± 3 Ma and
588 396 ± 4 Ma, Sunal 2012) located in the Sakarya Zone in NW Turkey that are suggested to
589 have an arc magmatic origin. The presence of a magmatic arc in close proximity to the
590 depositional site of the Halıcı Formation has previously been proposed by Eren (1993a) and
591 Kurt (1994). The presence of high amounts of feldspars (14%) and lithic sedimentary and
592 volcanic (12%) fragments in both samples is in accordance with this assumption (Table S2).
593 Internal structures of Devonian zircons from both samples revealed by cathodoluminescence
594 imaging share similarities with grains from the Karacabey Pluton (Sunal 2012) in terms of
595 pronounced oscillatory zoning and inherited cores and can be considered as a possible
596 source (see Supplementary Figure S2).
597
598 *5.2.2 Lower Mesozoic sediments*
599 The youngest analysed sediments from the Upper Triassic Ardıçlı Formation stand out with
600 largely unimodal age distribution spectra that record contribution from almost exclusively
601 Triassic and Upper Permian source rocks. In previous studies, rock fragments identified in
602 sediments of this formation were interpreted as being derived from both, the underlying
603 Sızma Group (including Kadınhanı metamagmatics) plus an unknown, more metamorphosed
604 source (Eren *et al.* 2004). In the light of our findings, we can exclude recycling of the
605 underlying rock units since their signature should be visible in the age spectra of the Ardıçlı
606 Formation. Triassic-aged zircons can have various origins, as evidence for Triassic igneous
607 activity is widespread in the Eastern Mediterranean region such as the Serbo-Macedonian
608 Massif (Himmerkus *et al.* 2009), the Pelagonian Zone (Anders *et al.* 2007), the Cyclades
609 (Tomaschek *et al.* 2001; Bröcker and Pidgeon 2007) or the Menderes Massif (Koralay *et al.*
610 2001). However, a very proximal provenance is likely and can be deduced from the high
611 proportion of (>75%) euhedral and angular zircon grains (Figure 10g, h). The closest
612 possible rocks that could have provided detritus to the Ardıçlı Formation are the Kadınhanı

613 metamagmatics of the Konya Complex itself. Recent U–Pb dating of zircon from
614 metatrachyandesites north of Konya yielded a Triassic age of 220.2 ± 0.7 Ma (Ustaömer *et al.*
615 2016b) and confirmed the previously published age of 221.6 ± 1.7 Ma (Güven *et al.* 2012).
616 Compositional data of zircons from sample T14-30, however, revealed remarkably high U
617 concentrations (average of 2300 ppm) and show that sediment cannot have been derived
618 from any of the above-mentioned occurrences. Unfortunately, no other rocks containing
619 zircons of corresponding age and composition could be identified in the larger study area.
620 Nonetheless, it has been demonstrated by Belousova *et al.* (2002) that the trace element
621 composition of zircon is sensitive to the type of source rock. Their study reveals a positive
622 correlation of U with incompatible elements like Y and other REE that consequently are
623 enriched in zircons from evolved granitoid rocks. Even though the second sample (T14-29)
624 reveals a very similar age spectrum, the zircons exhibit considerably lower amounts of U,
625 thus providing evidence that both samples do not share the same provenance. Thus we
626 assume that the sediment was supplied from a nearby source of evolved igneous rocks that
627 are not existent anymore or presently not exposed. Due to the very small difference between
628 crystallization ages of zircons and the depositional age of these sediments we suggest
629 volcanic rather than plutonic rocks as most likely sources. Even though granitic rocks may
630 have been exposed by rapid exhumation in an active tectonic setting.
631
632 ***5.3 Tectonic setting***
633 The chemical composition of sedimentary rocks is mainly controlled by the nature of their
634 source rocks but can subsequently be modified by secondary processes such as diagenesis,
635 weathering, sorting and/or recycling (McLennan *et al.* 1993). Even though the emphasis of
636 many geological studies is placed on the provenance of sedimentary rocks, it has become
637 common practice to utilize geochemical data for inferring tectonic settings of sedimentary
638 basins (e.g. Bhatia 1983; Bhatia and Crook 1986; Roser and Korsch 1986). However,
639 geochemical signatures cannot necessarily be assigned to a specific tectonic setting and it
640 has been shown that these approaches often do not provide satisfactory results or are

inconsistent with the regional geological framework or plate tectonic reconstructions (e.g. McLennan *et al.* 1990; Armstrong-Altrin and Verma 2005).

In this study, we used the conventional discrimination diagrams of Roser and Korsch (1986) and recently published discriminant function-based diagrams of Verma and Armstrong-Altrin (2013, 2016) to decipher the tectonic setting of the Konya basin (Figure 12, Table S3 in the Supplementary Material). Their new statistical approach was successfully tested on Neogene to Quarternary sediments from known tectonic settings and utilizes $\log_e$-ratio transformation of major (SiO_2, TiO_2, Al_2O_3, Fe_2O_3, MnO, MgO, CaO, Na_2O, K_2O and P_2O_5) and trace elements (Cr, Nb, Ni, V, Y and Zr). In addition to the geochemical data, we also used detrital zircon spectra of the studied samples (Figure 13). Following Cawood *et al.* (2012), the detrital zircon record of sedimentary rocks, in particular the difference between crystallization ages of zircon and the depositional age of the sediment reflects the nature of the depositional basin they were deposited in and allows for discrimination of convergent, collisional and extensional settings.

In the conventional diagram of Roser and Korsch (1986), the majority of our samples, as well as quartzites and psammites from the Halıcı Formation (analysed by Kurt 1996, 1997), are characterized by SiO_2, K_2O and Na_2O abundances typical for passive margin settings (Figure 12a, Table S3 in the Supplementary Material). With respect to the discriminant function-based diagrams, the sample population shows a larger spread (Figure 12b–d, Table S3 in the Supplementary Material). Samples from the mélange unit show a tendency towards a passive margin setting, the exception being the sedimentary block from the mélange (T14-34) that has a continental and oceanic island arc affinity. This is in accordance with detrital zircon data, suggesting an extensional setting for sedimentary matrix rocks (T14-20B and T14-31), but a convergent margin setting for the mélange block (Figure 13). In the ‘flysch’ unit, geochemical signatures of two highly mature samples (T14-22 and T14-23) point towards a passive margin setting, whereas data from two wackes (T14-36 and T14-39) are more ambiguous, slightly tending to an active setting (Figure 12). This is also inferred from the detrital zircon record, reflecting a passive margin setting (extensional) for the former and

669 an active margin setting (collisional) for the latter samples (Figure 13). Two out of three
670 samples from the Ardıçlı Formation plot in the 'Rift' and passive margin fields in every single
671 diagram whereas the conglomeratic sample (T14-30) shows active margin characteristics
672 (Figure 12). The detrital zircon record of both dated samples (T14-29 and T14-30) indicates a
673 convergent setting and documents high syndepositional igneous activity (Figure 13).
674 However, a passive margin setting is most likely and fits very well with previous
675 considerations, in which the Ardıçlı Formation was interpreted as synrift sequence related to
676 the opening of several back-arc oceans (e.g. Küre, Meliata, Pindos) during Triassic time in
677 response to Palaeotethyan slab roll-back (Eren *et al.* 2004).
678 With respect to the previous (palaeo)tectonic interpretations of the basin, an unambiguous
679 affinity to either northern Gondwana or southern Eurasia of the complex as a whole cannot
680 be established based on the available data. In fact, the Halıcı Formation has turned out as a
681 complex mixture of heterogeneous (mainly) sedimentary rocks that do not have a common
682 origin and reflect different depositional tectonic settings. The suite of samples that strongly
683 resembles Lower Palaeozoic sandstones of northern Gondwana reflects passive margin
684 signatures and does not document any input from an arc-derived material. Thus, certain
685 models proposing an active northern Gondwana margin (e.g. Özcan *et al.* 1988, 1990; Eren
686 and Kurt 2000; Robertson and Ustaömer 2009b) are not supported by our data. A possible
687 scenario, however, could involve short-lived or shallow-dipping southward subduction
688 beneath Gondwana without the formation of a major magmatic arc, as evidence for arc-
689 related magmatism on the Tauride domain is scarce (Figure 14a). Nonetheless,
690 Carboniferous arc-type magmatic rocks have been reported, for instance from the Simav
691 area of the northwestern Afyon Zone and the Cyclades and were interpreted as evidence for
692 southward subduction in Late Carboniferous–Early Permian time (e.g. Xypolias *et al.* 2006;
693 Candan *et al.* 2016). In contrast, samples documenting sediment supply (supposedly) from
694 units with a southern Eurasian affinity (i.e. T14-34, T14-36, T14-39) tend to have
695 compositional and geochemical features pointing to an active margin setting and contain
696 some arc-derived material (Figures 12). The high abundance of Devonian-aged zircons led

697 to suggests a magmatic arc could have developed during that time and was subsequently
698 uplifted and eroded in the Late Carboniferous–Early Permian. Results from the Ardıçlı
699 Formation indicate that subduction along a continental block with Eurasian affinity ceased
700 before Late Triassic time and a passive rift margin developed (Figure 14b).
701 In addition to the sedimentary sequences that were the focus of most studies, a large
702 number of igneous rocks from the Kadınhanı metamagmatics or volcano-sedimentary unit,
703 respectively, have been studied in the past decade as well (Eren *et al.* 2004; Göncüoğlu *et al.*
704 2007; Robertson and Ustaömer 2009b). Studied metavolcanic rocks and dykes exhibit arc-
705 and MORB-type characteristics and consistently show variable degrees of enrichment in
706 MORB-normalized trace element patterns in combination with (slightly) negative Nb
707 anomalies. These signatures were interpreted to document the initiation of a subduction
708 event in Carboniferous time, accompanied by the development of magmatic arc/fore-arc
709 sequences on the northern margin of Palaeotethys (Eren *et al.* 2004) or induced back-arc
710 rifting at the northern Gondwana margin, respectively (e.g. Göncüoğlu *et al.* 2007, Robertson
711 and Ustaömer 2009b). It should be noted that metatrachyandesites from the Kadınhanı and
712 Sızma areas, analysed by Göncüoğlu *et al.* (2007) have later been dated as Early Triassic by
713 Akal *et al.* (2012) and thus were probably related to rifting processes of a Neotethyan ocean.
714 In contrast, radiometric dating of metavolcanic rocks from the volcano-sedimentary unit
715 yielded Early Permian ages (Candan *et al.* 2009).
716 It remains to state that the complex structure and formation of the Upper Palaeozoic
717 sedimentary sequence (NW of Konya) is not yet fully understood. Impressions from the field
718 campaign already arose the question, whether the Halıcı Formation can be adequately
719 described as a single unit or, in fact, is composed of two or more subunits. Our initially
720 introduced subdivision into a mélange unit and a ‘flysch’ unit is primarily based on observed
721 differences in lithology, deformation and metamorphic degree. More specifically, studied
722 rocks from the mélange unit (in contrast to the ‘flysch’ unit) show phyllitic textures and
723 contain sigma-shaped quartz crystals witnessing relatively higher metamorphic conditions
724 that allow ductile deformation. Also, the presented data have shown considerable differences

725 in terms of composition and provenance within a supposedly single formation. In any case,
726 we conclude that the final assembly of the formation must have been completed until Late
727 Triassic time, as it is unconformably overlain by the Upper Triassic Ardıçlı Formation.
728
729 ***5.4 Comparable units***
730 The studied area has often been compared to Palaeotethys-related units on the Karaburun
731 Peninsula in western Turkey and on the Aegean island of Chios (e.g. Eren *et al.* 2004;
732 Robertson and Ustaömer 2011) (Figure 1a). On the Karaburun Peninsula, the Palaeozoic
733 succession is mainly composed of siliciclastic sedimentary rocks of Pennsylvanian–
734 Cisuralian age (Löwen *et al.* 2017). It comprises low-grade metamorphosed sandstones and
735 shales (Küçükbahçe Formation) and a mélange unit with Silurian–Carboniferous blocks of
736 black chert, pelagic limestones and poorly dated volcanic rocks that are embedded in a
737 highly deformed siliciclastic matrix (Dikendağı Formation) (Kozur 1997, 1998; Çakmakoğlu
738 and Bilgin 2006). The Dikendağı Formation is intruded by two Early Triassic granitoid bodies
739 that yielded a biotite Rb–Sr isochron age of 239.9 ± 2.4 Ma (Ercan *et al.* 2000) and zircon U–
740 Pb ages of 244.4 ± 1.5 Ma (Ustaömer *et al.* 2016b) and 247.1 ± 2.0 Ma, respectively (Akal *et*
741 *al.* 2011). Previous studies revealed an arc-related geochemical signature for these rocks
742 and document ongoing subduction during that period. The Palaeozoic sequence is
743 unconformably overlain by a thick, carbonate-dominated sequence of Early Triassic to Late
744 Cretaceous age (Çakmakoğlu and Bilgin 2006). On Chios, the mélange is part of the
745 'autochthonous' Lower Unit and comprises a mid-Carboniferous siliciclastic matrix with
746 blocks of limestone, radiolarites and volcanic rocks of Silurian to Carboniferous age
747 (Meinhold *et al.* 2008b). The Lower Unit is tectonically overlain by an 'allochthonous' Upper
748 Unit of Late Carboniferous to Jurassic age (Besenecker *et al.* 1968; Meinhold *et al.* 2007,
749 2008b). In contrast to the Konya Complex, a Silurian–Devonian carbonate platform is absent
750 in both localities and Palaeozoic limestones exclusively occur as blocks in the mélange units.
751 All these areas play an important role in geodynamic reconstructions in a period of time when
752 the Palaeotethys diminished in size and finally vanished. Previously, the tectono-stratigraphic

753 similarities of the Chios, Karaburun and Konya units were used as strong arguments to
754 correlate these units and interpret them as different parts of the same active continental
755 margin (Robertson and Ustaömer 2009b). Essential provenance data to test if this correlation
756 is viable were scarce but were provided over the last years for both, Chios and Karaburun
757 (Meinhold *et al.* 2007, 2008a, b; Löwen *et al.* 2017, 2018). These studies have identified low-
758 grade metamorphosed sedimentary rocks as major sources but locally also recognized high
759 proportions of (sub)angular grains derived from a felsic volcanic source that was interpreted
760 as an indication for the presence of a relatively proximal continental-arc. Similar to Konya,
761 compositional data of detrital rutile are indicative of amphibolite- to eclogite-facies rocks.
762 Nevertheless, a considerable amount (up to 25%) of high-temperature rutiles in the
763 Dikendağı Formation implies the existence of high-grade (granulite-facies) rocks in the
764 source area. In terms of source rock composition, detrital rutiles from the Upper Palaeozoic
765 rocks of Karaburun were (with few exceptions) dominantly derived from felsic lithologies,
766 which is also recorded by grains from the Permian–Carboniferous and Permian–Triassic
767 units of Chios (Meinhold *et al.* 2008a; Löwen *et al.* 2018). Despite the many similarities,
768 detrital garnet and Cr-spinel do only occur in the Chios–Karaburun units, while they are
769 virtually absent in studied rocks from the Konya Complex. In the Upper Palaeozoic units, the
770 compositions of Cr-spinel indicate a mixed (ultra)mafic source of predominantly harzburgite
771 and minor lherzolite composition. In contrast, euhedral Cr-spinel extracted from Lower
772 Triassic siliciclastic rocks of the Karaburun Peninsula (Gerence Formation) exhibit
773 significantly higher Cr- and Mg-numbers and were interpreted as being derived from
774 podiform chromitites related to an intra-oceanic back-arc setting above a supra-subduction
775 zone within the Palaeotethys (Löwen *et al.* 2018). Furthermore, the detrital zircon record of
776 sandstones from Chios and Karaburun provided a substantial piece of information for
777 palaeogeographic considerations. Their age spectra were dominated by Palaeozoic to
778 Neoproterozoic zircons, but locally contained large Ordovician–Devonian populations. It was
779 concluded that most of the Carboniferous–Triassic successions were deposited along the
780 southern active margin of a continental block with Eurasian affinity in a continental-arc

781 environment, and their source areas should probably be sought in basement rocks of units
782 located along this margin (e.g. Sakarya Zone, present-day Balkan region) (Meinhold *et al.*
783 2008b; Löwen *et al.* 2017). Nevertheless, detrital zircon spectra of a few samples from the
784 Karaburun mélange closely resemble Palaeozoic and Mesozoic siliciclastic rocks from the
785 northern Gondwana margin (Meinhold *et al.* 2011; 2013; Dörr *et al.* 2015) and show great
786 similarities with samples from the Palaeozoic Konya Complex as well (T14-20B, T14-22 and
787 T14-31).
788 In summary, the discussed units do not only have comparable tectono-stratigraphic
789 structures but, partially, do also share a similar provenance. Available data from the Chios–
790 Karaburun units on the one hand mainly favour an assignment to an active margin of
791 Eurasian affinity in Late Palaeozoic time. Data from time-equivalent deposits of the Konya
792 Complex on the other hand record sediment supply from units of both, Eurasia-related and
793 Gondwana-related. Future tectonometamorphic and structural studies are necessary to fully
794 understand the formation of the Konya Complex and adjust the palaeoposition of these rocks
795 within the Tethyan realm.
796
797 **6. Conclusions**
798 The new data from siliciclastic rocks of the Upper Palaeozoic Konya Complex and its
799 Mesozoic cover sequence give insight on the depositional history of the Konya basin and
800 shed light on their age, composition and origin. The most important findings can be
801 summarized as followed:
802
803 - The Halıcı Formation is not considered as a single overall unit but can be divided into
804 (several) subunits, such as a low-grade ‘flysch’ unit (e.g. mudstones, siltstones,
805 sandstones) and a slightly more metamorphosed, block-bearing mélange unit (e.g.
806 sandstones, conglomerates, cherts), representing the actual mélange.
807 - Provenance sensitive elements and mineral chemical data of rutile from the Ardıçlı
808 and Halıcı formations document sediment supply from predominantly amphibolite- to

eclogite-facies rocks of felsic character. Evidence for input from metamafic source rocks is rare.

- The youngest populations of detrital zircons indicate an Early Palaeozoic depositional age for the Halıcı Formation. But given the available biostratigraphic data from the matrix rocks and embedded limestone blocks, we assume that sediment accumulation in Pennsylvanian–Cisuralian time, contemporaneously to the Karaburun mélange is most likely.
- Sandstones of this formation revealed significantly different detrital zircon age spectra and document sediment supply from units of both, southern Eurasian affinity (i.e. Sakarya Zone, Sredna Gora Zone, Serbo-Maedonian Massif) and northern Gondwanan affinity (i.e. Saharan Metacraton, Arabian–Nubian Shield).
- Samples with a (supposed) Eurasian affinity are characterized by prominent Silurian–Devonian and Ordovician–Silurian populations. We assume that large volumes of detritus were derived from felsic igneous bodies related to arc magmatic activity due to ongoing subduction beneath Eurasia-related continental blocks.
- The provenance of Late Triassic sandstones from the Ardıçlı Formation remains enigmatic. Our data clearly indicate a very proximal source and exclude recycling of material from the underlying formations of the Sızma Group.

Acknowledgements

We gratefully acknowledge financial support from the German Research Foundation (DFG, grant number ME 3882/3-1) and the Göttingen University start-up funding for young academics (grant to GM). We thank Gerald Hartmann for XRF analysis, Klaus Simon for ICP-MS analysis, and Andreas Kronz for providing access to the EMPA. Finally, we are grateful to Vasileios Chatzaras, Alastair H. F. Robertson and an anonymous reviewer for their constructive comments which helped to improve the original manuscript, and to Robert J. Stern for his careful editorial handling.

Disclosure statement

No potential conflict of interest was reported by the authors.

Funding

This work was supported by the German Research Foundation [ME 3882/3-1]; and the Göttingen University start-up funding for young academics [Grant to GM].

ORCID

Guido Meinhold, https://orcid.org/0000-0001-8375-8375

Arzu Arslan, https://orcid.org/0000-0002-1556-9166

References

Abbo, A., Avigad, D., Gerdes, A., and Güngör, T., 2015, Cadomian basement and Paleozoic to Triassic siliciclastics of the Taurides (Karacahisar dome, south-central Turkey): Paleogeographic constraints from U–Pb–Hf in zircons: Lithos, v. 227, p. 122–139.

Akal, C., Candan, O., Koralay, O., Öberhänsli, R., Chen, F., and Prelević, D., 2012, Early Triassic potassic volcanism in the Afyon Zone of the Anatolides/Turkey: implications for the rifting of the Neo-Tethys: International Journal of Earth Sciences, v. 101, p. 177–194.

Anders, B., Reischmann, T., and Kostopoulos, D., 2007, Zircon geochronology of basement rocks from the Pelagonian zone, Greece: constraints on the pre-Alpine evolution of the westernmost internal Hellenides: International Journal of Earth Sciences, v. 96, p. 639–661.

Armstrong-Altrin, J.S., and Verma, S.P., 2005, Critical evaluation of six tectonic setting discrimination diagrams using geochemical data of Neogene sediments from known tectonic settings: Sedimentary Geology, v. 177, p. 115–129.

Avigad, D., Kolodner, K., McWilliams, M., Persing, H., and Weissbrod, T., 2003, Origin of northern Gondwana Cambrian sandstone revealed by detrital zircon SHRIMP dating:

Geology, v. 331, p. 227–230.

Avigad, D., Gerdes, A., Morag, N., and Bechstädt, T., 2012, Coupled U–Pb–Hf of detrital zircons of Cambrian sandstones from Morocco and Sardinia: implications for provenance and Precambrian crustal evolution of North Africa: Gondwana Research, v. 21, p. 690–703.

Be'eri-Shlevin, Y., Katzir, Y., Whitehouse, M.J., and Kleinhanns, I.C., 2009, Contribution of pre Pan-African crust to formation of the Arabian Nubian Shield: new secondary ionization mass spectrometry U–Pb and O studies of zircon: Geology, v. 37, p. 899–902.

Belousova, E., Griffin, W., O'Reilly, S.Y., and Fisher, N., 2002, Igneous zircon: trace element composition as an indicator of source rock type. Contribution to Mineralogy and Petrology, v. 143, p. 602–622.

Besenecker, H., Dürr, S., Herget, G., Jacobshagen, V., Kauffmann, G.L., Lüdtke, G., Roth, W., and Tietze, K.W., 1968, Geologie von Chios (Ägäis): Geologica et Palaeontologica, v. 2, 121–150.

Bhatia, M.R., 1983, Plate tectonics and geochemical composition of sandstones: The Journal of Geology, v. 91, p. 611–627.

Bhatia, M.R., and Crook, A.W., 1986, Trace element characteristics of graywackes and tectonic setting discrimination of sedimentary basins. Contributions to Mineralogy and Petrology, v. 92, p. 181–193.

Boynton, W.V., 1984, Geochemistry of the rare earth elements: Meteorite studies, *in* Henderson, P., ed., Geochemistry of the Rare Earth Elements: Elsevier, p. 63–114.

Bracciali, L., Marroni, M., Pandolfi, L., and Rocchi, S., 2007, Geochemistry and petrography of Western Tethys Cretaceous sedimentary covers (Corsica and Northern Apennines): From source areas to configuration of margins, *in* Arribas, J., Critelli, S., and Johnsson, M.J., eds., Sedimentary Provenance and Petrogenesis: Perspectives from Petrography and Geochemistry: Geological Society of America, Special Paper, v. 420, p. 73–93.

890 Bröcker, M., and Pidgeon, R.T., 2007, Protolith ages of meta-igneous and metatuffaceous
891 rocks from the Cycladic Blueschist unit, Greece: results of a reconnaissance U–Pb
892 zircon study: The Journal of Geology, v. 115, p. 83–98.

893 Çakmakoğlu, A., and Bilgin, Z., 2006, Pre-Neogene stratigraphy of the Karaburun Peninsula
894 (W of İzmir Turkey): Bulletin of he Mineral Research and Exploration, v. 132, 33–61.

895 Candan, O., Dora, O., Oberhänsli, R., Çetinkaplan, M., Partzsch, J., Warkus, F., and Dürr, S.,
896 2001, Pan-African high-pressure metamorphism in the Precambrian basement of the
897 Menderes Massif, western Anatolia, Turkey: International Journal of Earth Sciences, v.
898 89, p. 793–811.

899 Candan, O., Oberhänsli, R., Akal, C., Koralay, O.E., Pourteau, A., and Çetinkaplan, M., 2009,
900 Stratigraphy and Alpine metamorphism of the Afyon Zone. 62nd Geological Kurultai of
901 Turkey, 13–17 April 2009, MTA Ankara, Turkey, Abstract, p. 32–33.

902 Candan, O., Akal, C., Koralay, O.E., Okay, A.I., Oberhänsli, R., Prelević, D., and Mertz-Kraus,
903 R., 2016, Carboniferous granites on the northern margin of Gondwana, Anatolide-
904 Tauride Block, Turkey – Evidence for southward subduction of Paleotethys:
905 Tectonophysics, v. 683, p. 349–366.

906 Cawood, P.A., Hawkesworth, C.J., and Dhuime, B., 2012, Detrital zircon record and tectonic
907 setting: Geology, v. 40, p. 875–878.

908 Chatzaras, V., Dörr, W., Gerdes, A., Krahl, J., Xypolias, P., and Zulauf, G., 2016, Tracking
909 the late Paleozoic to early Mesozoic margin of northern Gondwana in the Hellenides:
910 paleotectonic constraints from U–Pb detrital zircon ages: International Journal of Earth
911 Sciences, v. 105, p. 1881–1899.

912 Daşçı, H.T., Parlak, O., Nurlu, N., and Billor, Z., 2015, Geochemical characteristics and age
913 of metamorphic sole rocks within a Neotethyan ophiolitic mélange from Konya region
914 (central southern Turkey): Geodinamica Acta, v. 27, p. 223–243.

915 Dott, R.H., 1964, Wacke, graywacke and matrix; what approach to immature sandstone
916 classification?: Journal of Sedimentary Petrology, v. 34, p. 625–632.

917 Dörr, W., Zulauf, G., Gerdes, A., Lahaye, Y., Kowalczyk, G., 2015, A hidden Tonian
918 basement in the eastern Mediterranean: Age constraints from U–Pb data of magmatic
919 and detrital zircons of the external Hellenides (Crete and Peloponnesus): Precambrian
920 Research, v. 258, p. 83–108.

921 Eren, Y., 1993a, The geology of the Eldeğ-Derbent-Tepeköy-Söğütözü (Konya) region: [PhD
922 thesis]: Selçuk University Konya (Unpublished), 224 p.

923 Eren, Y., 1993b, Stratigraphy of autochthonous and cover units of the Bozdağlar massif NW
924 Konya: Geological Bulletin of Turkey, v. 36, p. 7–23.

925 Eren, Y., 1996, Stratigraphy and geological evolution of the Bozdağlar Massif in the south of
926 Ilgın and Sarayönü (Konya), *in* Kormaz, S., and Akçay, M., eds., Karadeniz Technical
927 University Department of Geology 30th Year Symposium, Proceedings, II, p. 694–707 (in
928 Turkish with English abstract).

929 Eren, Y., and Kurt, H., 2000, The stratigraphical, geochemical and geodynamical modelling
930 of the northeast margin of Menderes-Taurus Block: Journal of the Faculty of
931 Engineering and Architecture, Selçuk University, Konya, v. 15, p. 25–41.

932 Eren, Y., 2001, Polyphase alpine deformation at the northern edge of the Menderes-Taurus
933 block, North Konya, central Turkey: Journal of Asian Earth Sciences, v. 19, p. 737–749.

934 Eren, Y., Kurt, H., Rosselet, F., and Stampfli, G.M., 2004, Palaeozoic deformation and
935 magmatism in the northern area of the Anatolide block (Konya), witness of the
936 Palaeotethys active margin: Eclogae Geologicae Helvetiae, v. 97, p. 293–306.

937 Göğer, E., and Kıral, K., 1969, Geology of the Kızılören region: Mineral Research and
938 Exploration Institute of Turkey (MTA), Report No. 5204, Ankara (in Turkish).

939 Göncüoğlu, C., and Kozur, H.W., 1998, Remarks to the pre-Variscan development in Turkey,
940 *in* Linnemann, U., Heuse, T., Fatka, O., Kraft, P., Brocke, R., and Erdtmann, B., eds.,

941 Pre-Variscan terrane analysis of ‘‘Gondwanan Europe”: Staatliche Naturhistorische
942 Sammlungen Dresden, Museum für Mineralogie und Geologie, Dresden, v. 9, p. 137–
943 138.

944 Göncüoğlu, M.C., Kozur, H.W., Turhan, N., and Göncüoğlu, Y., 2000, Stratigraphy of the
945 Silurian–Lower Carboniferous rock units in Konya area, *in* VIII International Meeting of
946 IGCP 421 in 1st Congresso Iberico de Paleontologia, Evora, p. 227–228.

947 Göncüoğlu, M.C., Çapkınoğlu, Ş., Gürsu, S., Noble, P., Turhan, N., Tekin, U.K., Okuyucu, C.,
948 and Göncüoğlu, Y., 2007, The Mississippian in the Central and Eastern Taurides
949 (Turkey): constraints on the tectonic setting of the Tauride–Anatolide Platform:
950 Geologica Carpathica, v. 58, p. 427–442.

951 Güven, A., Ustaömer, T., and Peytcheva, I., 2012, Late Triassic crustal extension in NW
952 Konya (Afyon Zone): new findings from LA-ICP-MS U–Pb zircon dating of the Ladik
953 Dyke Swarm and the Kadınhanı meta-volcanics, *in* Proceedings of the 5th
954 Geochemistry Symposium, 23–25 May 2012, Pamukkale University, Denizli-Turkey, p.
955 122–123.

956 Herron, M.M., 1988, Geochemical classification of terrigenous sands and shales from core or
957 log data: Journal of Sedimentary Petrology, v. 58, p. 820–829.

958 Himmerkus, F., Reischmann, T., and Kostopoulos, D., 2009, Triassic rift-related meta-
959 granites in the internal Hellenides, Greece: Geological Magazine, v. 146, p. 252–265.

960 Jacobshagen, V., 1986, Geologie von Griechenland: Berlin, Gebrüder Borntraeger, 363 p.

961 Johnson, P.R., and Woldehaimanot, B., 2003, Development of the Arabian–Nubian Shield:
962 perspectives on accretion and deformation in the northern East African Orogen and the
963 assembly of Gondwana. *in* Yoshida, M., Windley, B.F., and Dasgupta, S., eds.,
964 Proterozoic East Gondwana: Supercontinent Assembly and Breakup: Geological
965 Society London, Special Publications, v. 206, p. 289–325.

966 Johnsson, M.J., 1993, The system controlling the composition of clastic sediments. *in*

967 Johnsson, M.J., and Basu, A., eds., Processes Controlling the Composition of Clastic
968 Sediments: Geological Society of America, Special Papers, v. 284, p. 1–19.

969 Karaman, M.E., 1986, The geology and tectonic evolution of the Altınekin (Konya) region:
970 Geological Bulletin of Turkey, v. 29, p. 157–171.

971 Kolodner, K., Avigad, D., McWilliams, M., Wooden, J.L., Weissbrod, T., and Feinstein, S.,
972 2006, Provenance of north Gondwana Cambrian–Ordovician sandstone: U–Pb SHRIMP
973 dating of detrital zircons from Israel and Jordan: Geological Magazine, v. 143, p. 367–
974 391.

975 Koralay, O.E., Satir, M., and Dora, O.Ö., 2001, Geochemical and geochronological evidence
976 for Early Triassic calc-alkaline magmatism in the Menderes Massif, western Turkey:
977 International Journal of Earth Sciences, v. 89, p. 822–835.

978 Kozur, H., 1997, First discovery of Muellerisphaerida (inc. sedis) and *Eoalbaillella*
979 (Radiolaria) in Turkey and the age of the siliciclastic sequence (clastic series) in
980 Karaburun peninsula: Freiberger Forschungshefte Reihe C Geowissenschaften, v. 46, p.
981 33–59.

982 Kozur, H., 1998, The age of the siliciclastic series (“Karareis formation”) of the western
983 Karaburun peninsula, western Turkey, *in* Szaniawski, H., ed., Proceedings of the Sixth
984 European Conodont Symposium (ECOS VI): Palaeontologia Polonica, v. 58, p. 171–
985 189.

986 Kozur, H.W., 1999, A review of the systematic position and stratigraphic value of
987 Muellerisphaerida, *in* Tongiorgi, M., and Palyford, G. eds., Studies in Palaeozoic
988 palynology. Selected papers from the CIMP Symposium at Pisa, 1998: Bolletino della
989 Societa Paleontologia Italiano, v. 38, p. 197–206.

990 Kurt, H., 1994, Petrography and Geochemistry of Kadınhanı (Konya) area, Central Turkey
991 [PhD thesis]: Glasgow University (Unpublished), U.K., 191 p.

992 Kurt, H., 1996, Geochemical characteristics of the meta-igneous rocks near Kadınhanı
993 (Konya), Turkey: Geosound, v. 28, p. 1–22.

994 Kurt, H., 1997, Geochemistry of metasedimentary rocks of the Kadınhanı (Konya) area,
995 Turkey: Geosound, v. 31, p. 1–21.

996 Löwen, K., Meinhold, G., Güngör, T., and Berndt, J., 2017, Palaeotethys-related sediments
997 of the Karaburun Peninsula, western Turkey: constraints on provenance and
998 stratigraphy from detrital zircon geochronology: International Journal of Earth Sciences,
999 v. 8, p. 2771–2796.

1000 Löwen, K., Meinhold, G., and Güngör, T., 2018, Provenance and tectonic setting of
1001 Carboniferous–Triassic sandstones from the Karaburun Peninsula, western Turkey: A
1002 multi-method approach with implications for the Palaeotethys evolution: Sedimentary
1003 Geology, v. 375, p. 232–255.

1004 Marsellos, A.E., Foster, D.A., Kamenov, G.D., and Kyriakopoulos, K., 2012, Detrital zircon U-
1005 Pb data from the Hellenic south Aegean belts: constraints on the age and source of the
1006 South Aegean basement: Journal of the Virtual Explorer, doi:10.3809/jvirtex.2011.00284.

1007 McLennan, S.M., Taylor, S.R., McCulloch, M.T., and Maynard, J.B., 1990, Geochemical and
1008 Nd–Sr isotopic composition of deep-sea turbidites: crustal evolution and plate tectonic
1009 associations: Geochimica et Cosmochimica Acta, v. 54, p. 2015–2050.

1010 McLennan, S.M., Hemming, S., McDaniel, D.K., and Hanson, G.N., 1993, Geochemical
1011 approaches to sedimentation, provenance, and tectonics, *in* Johnsson, M.J., and Basu,
1012 A., eds., Processes Controlling the Composition of Clastic Sediments: Geological
1013 Society of America, Special Papers, v. 284, p. 21–40.

1014 Meinhold, G., Kostopoulos, D., Reischmann, T., 2007, Geochemical constraints on the
1015 provenance and depositional setting of sedimentary rocks from the islands of Chios,
1016 Inousses and Psara, Aegean Sea, Greece: implications for the evolution of
1017 Palaeotethys: Journal of the Geological Society, v. 164, p. 1145–1163.

1018 Meinhold, G., Anders, B., Kostopoulos, D., and Reischmann, T., 2008a, Rutile chemistry and
1019 thermometry as provenance indicator: An example form Chios Island, Greece:
1020 Sedimentary Geology, v. 203, p. 98–111.

1021 Meinhold, G., Reischmann, T., Kostopoulos, D., Lehnert, O., Matukov, D., and Sergeev, S.,
1022 2008b, Provenance of sediments during subduction of Palaeotethys: detrital zircon ages
1023 and olistolith analysis in Palaeozoic sediments from Chios Island, Greece:
1024 Palaeogeography, Palaeoclimatology, Palaeoecology, v. 263, p. 71–91.

1025 Meinhold, G., and Frei, D., 2008, Detrital zircon ages from the islands of Inousses and Psara,
1026 Aegean Sea, Greece: constraints on depositional age and provenance: Geological
1027 Magazine, v. 145, p. 886–891.

1028 Meinhold, G., 2010, Rutile and its applications in earth sciences: Earth-Science Reviews, v.
1029 102, p. 1–28.

1030 Meinhold, G., Morton, A.C., Fanning, C.M., Frei, D., Howard, J.P., Philips, R.J., Strogen, D.,
1031 and Whitham, A.G., 2011, Evidence from detrital zircons for recycling of
1032 Mesoproterozoic and Neoproterozoic crust recorded in Paleozoic and Mesozoic
1033 sandstones of southern Libya: Earth and Planetary Science Letters, v. 312, p. 164–175.

1034 Meinhold, G., Morton, A.C., and Avigad, D., 2013, New insights into peri-Gondwana
1035 paleogeography and the Gondwana super-fan system from detrital zircon U–Pb ages:
1036 Gondwana Research, v. 23, p. 661–665.

1037 Mitchell, A.H.G., and Reading, H.G., 1986, Sedimentation and tectonics, *in* Reading, H.G.,
1038 ed., Sedimentary environments and facies: 2nd edition, Blackwell, Oxford, p. 471–519.

1039 Moix, P., Beccaletto, L., Kozur, H.W., Hochard, C., Rosselet, F., and Stampfli, G.M., 2008, A
1040 new classification of the Turkish terranes and sutures and its implication for the
1041 paleotectonic history of the region: Tectonophysics, v. 451, p. 7–39.

1042 Morton, A.C., 1985, Heavy minerals in provenance studies, *in* Zuffa, G.G., ed., Provenance
1043 of Arenites: Reidel, Dordrecht, p. 249–277.

1044 Okay, A.I., Satir, M., Maluski, M., Siyako, M., Monie, P., Metzger, R., and Akyüz, S., 1996,
1045 Palaeo- and Neo-Tethyan events in northwestern Turkey: geologic and geochronologic
1046 constraints, *in* Yin, A., and Harrison, T.M., ed., The tectonic evolution of Asia:
1047 Cambridge University Press, p. 420–441.

1048 Okay, A.I., and Tüysüz, O., 1999, Tethyan sutures of northern Turkey, *in* Durand, B., Jolivet,
1049 L., Horivath, F., and Séranne, M., eds., The Mediterranean Basin: Tertiary extension
1050 within the Alpine Orogen: Geological Society London, Special Publications, v. 156, p.
1051 475–515.

1052 Okay, A.I., Satir, M., and Siebel, W., 2006, Pre-Alpide Palaeozoic and Mesozoic orogenic
1053 events in the Eastern Mediterranean region, *in* Gee, D.G., and Stephenson, R.A., eds.,
1054 European lithosphere dynamics: Geological Society London, Memoirs, v. 32, p. 389–
1055 405.

1056 Okay, A.I., Satır, M., and Shang, C.K., 2008, Ordovician metagranitoid from the Anatolide-
1057 Tauride block, northwest Turkey: geodynamic implications: Terra Nova, v. 20, p. 280–
1058 288.

1059 Özbey, Z., Ustaömer, T., Robertson, A.H.F., and Ustaömer, P.A., 2013, Tectonic significance
1060 of Late Ordovician granitic magmatism and clastic sedimentation on the northern margin
1061 of Gondwana (Tavsanli Zone, NW Turkey): Journal of the Geological Society, v. 170, p.
1062 159–173.

1063 Özcan, A., Göncüoğlu, M.C., Turhan, N., Uysal, S., Şentürk, K., and Işık, A., 1988, Late
1064 Palaeozoic evolution of the Kütahya-Bolkardağ Belt: METU Journal of Pure and Applied
1065 Science, v. 21, p. 211–220.

1066 Özcan, A., Göncüoğlu, M.C., Turhan, N., Uysal, S., Işık, A., and Şentürk, K., 1990, Geology
1067 of the basement rocks of the Konya-Kadınhanı-Ilgın region: Mineral Research and
1068 Exploration Institute of Turkey (MTA), Report No. 9535, Ankara (in Turkish).

1069 Özmen, F., and Reischmann, T., 1999, The age of the Sakarya continent in W Anatolia:
1070 implications for the evolution of the Aegean region: Journal of Conference Abstracts, v.
1071 4, p. 805.

1072 Peytcheva, I., and von Quadt, A., 2004, The Palaeozoic protoliths of the Central Srednogorie,
1073 Bulgaria: records in zircons from basement rocks and Cretaceous magmatites: 5th
1074 ISEMG Conference Proceedings, v. 1, p. 392–395.

1075 Robertson, A.H.F., and Ustaömer, T., 2009a, Upper Palaeozoic subduction/accretion
1076 processes in the closure of Palaeotethys: evidence from the Chios Melange (E Greece),
1077 the Karaburun Melange (W Turkey) and the Teke Dere Unit (SW Turkey): Sedimentary
1078 Geology, v. 220, p. 29–59.

1079 Robertson, A.H.F., and Ustaömer, T., 2009b, Formation of the Late Palaeozoic Konya
1080 Complex and comparable units in southern Turkey by subduction–accretion processes:
1081 Implications for the tectonic development of Tethys in the Eastern Mediterranean
1082 region: Tectonophysics, v. 473, p. 113–148.

1083 Robertson, A.H.F., and Ustaömer, T., 2011, Role of tectonic-sedimentary melange and
1084 Permian–Triassic cover units, central southern Turkey in Tethyan continental margin
1085 evolution: Journal of Asian Earth Sciences, v. 40, p. 98–120.

1086 Romano, S.S., Dörr, W., and Zulauf, G., 2004, Significant Pb loss of Cadomian zircons due
1087 to Alpine subduction of pre-Alpine basement of eastern Crete (Greece): International
1088 Journal of Earth Sciences, v. 93, p. 844–859.

1089 Roser, B.P., and Korsch, R.J., 1986, Determination of tectonic setting of sandstone–
1090 mudstone suites using SiO_2 content and K_2O/Na_2O ratio. The Journal of Geology, v. 94,
1091 p. 635–650.

1092 Rudnick, R.L., and Gao, S., 2003, Composition of the continental crust: Treatise on
1093 Geochemistry, v. 3, p. 1–64.

1094 Şengör, A.M.C., and Yılmaz, Y., 1981, Tethyan evolution of Turkey: a plate tectonic

approach: Tectonophysics, v. 75, p. 181–241.

Şengör, A.M.C., Yilmaz, Y., and Sungurlu, O., 1984, Tectonics of the Mediterranean Cimmerides: nature and evolution of the western termination of Palaeo-Tethys, *in* Dixon, J.E., and Robertson, A.H.F., eds., The Geological Evolution of the Eastern Mediterranean: Geological Society London, Special Publications, v. 17, p. 77–112.

Sestini, G., 1970, Flysch facies and turbidite sedimentology: Sedimentary Geology, v. 4, p. 559–597.

Stampfli, G.M., Mosar, J., Favre, P., Pillevuit, A., and Vannay, J.-C., 2001a, Permo-Mesozoic evolution of the western Tethyan realm: the Neotethys/East-Mediterranean connection, *in* Ziegler, P.A., Cavazza, W., Robertson, A.H.F., and Crasquin-Soleau, S. eds., Peri-Tethys memoir 6: Peri-Tethyan rift/wrench basins and passive margins, IGCP 369: Mémoires du Muséum National d'Histoire Naturelle, v. 186, p. 51–108.

Stampfli, G.M., Borel, G., Cavazza, W., Mosar, J., and Ziegler, P.A., eds., 2001b, The Palaeotectonic atlas of the Peritethyan domain. CD ROM; European Geophysical Society

Stampfli, G.M., and Borel, G., 2002, A plate tectonic model for the Paleozoic and Mesozoic constrained by dynamic plate boundaries and restored synthetic oceanic isochrones: Earth and Planetary Science Letters, v. 196, p. 17–33.

Sunal, G., 2012, Devonian magmatism in the western Sakarya Zone, Karacabey region, NW Turkey: Geodinamica Acta, v. 25, p. 183–201.

Taylor, S.R., and McLennan, S.H., 1985, The Continental Crust: Its Composition and Evolution: Blackwell, Oxford, 312 p.

Titorenkova, R., Macheva, L., Zidarov, N., von Quadt, A., and Peytcheva, I., 2003, Metagranites from SW Bulgaria as a part of the Neoproterozoic to early Paleozoic system in Europe: new insight from zircon typology U–Pb isotope data Hf-tracing: Geophysical Research Abstracts, v. 5, abs. 08963.

1121 Tomaschek, F., Kennedy, A., Keay, S., and Ballhaus, C., 2001, Geochronological constraints
1122 on Carboniferous and Triassic magmatism in the cyclades: SHRIMP U–Pb ages of
1123 zircons from Syros, Greece: Journal of Conference Abstracts, v. 6, p. 315.

1124 Tomkins, H.S., Powell, R., and Ellis, D.J., 2007, The pressure dependence of the zirconium-
1125 in-rutile thermometer: Journal of Metamorphic Geology, v. 25, p. 703–713.

1126 Triebold, S., von Eynatten, H., and Zack, T., 2012, A recipe for the use of rutile in
1127 sedimentary provenance analysis: Sedimentary Geology, v. 282, p. 268–275.

1128 Ustaömer, T., Ustaömer, P.A., Robertson, A.H.F., and Gerdes, A., 2016a, Testing alternative
1129 tectonic models of Palaeotethys in the E Mediterranean region: new U-Pb and Lu-Hf
1130 isotopic analyses of detrital zircons from Late Carboniferous and Late Triassic
1131 sandstones associated with the Anatolide and Tauride blocks (S Turkey): EGU General
1132 Assembly 2016, Geophysical Research Abstracts, v. 18, EGU2016-15469-1.

1133 Ustaömer, T., Ustaömer, P.A., Robertson, A.H.F., and Gerdes, A., 2016b, Implications of U–
1134 Pb and Lu–Hf isotopic analysis of detrital zircons for the depositional age, provenance
1135 and tectonic setting of the Permian–Triassic Palaeotethyan Karakaya Complex, NW
1136 Turkey: International Journal of Earth Sciences, v. 105, p. 7–38.

1137 Ustaömer, T., Ustaömer, P.A., Robertson, A.H.F., and Gerdes, A., 2018, U-Pb and Lu-Hf
1138 isotopic data from detrital zircons in Late Carboniferous and Late Triassic sandstones
1139 used to determine provenance and test alternative tectonic models of the tectonic
1140 setting of the Anatolide and Taurides, S Turkey: Abstracts, GeoBonn 2018, 2–6th 2018,
1141 Bonn, Germany, p. 65.

1142 Verma, S.P., and Armstrong-Altrin, J.S., 2013, New multi-dimensional diagrams for tectonic
1143 discrimination of siliciclastic sediments and their application to Precambrian basins:
1144 Chemical Geology, v. 355, p. 117–133.

1145 Verma, S.P., and Armstrong-Altrin, J.S., 2016, Geochemical discrimination of siliciclastic
1146 sediments from active and passivemargin settings: Sedimentary Geology, v. 332, p. 1–

12.

von Raumer, J., Stampfli, G.M., Borel, G., and Bussy, F., 2002, Organizationn of pre-Variscan basement areas at the North-Gondwanan margin: International Journal of Earth Sciences, v. 91, p. 35–52.

Wiesner, K., 1968, Konya mercury deposits and studies on them: Mineral Research and Exploration Bulletin, v. 70, p. 178–213.

Xypolias, P., Dörr, W., and Zulauf, G., 2006, Late Carboniferous plutonism within the pre-Alpine basement of the External Hellenides (Kithira, Greece): evidence from U–Pb zircon dating: Journal of the Geological Society, v. 163, p. 539–547.

Zack, T., Moraes, R., and Kronz, A., 2004, Temperature dependence of Zr in rutile: empirical calibration of a rutile thermometer: Contributions to Mineralogy and Petrology, v. 148, p. 471–488.

Zulauf, G., Dörr, W., Fischer-Spurlock, S.C., Gerdes, A., Chatzaras, V., and Xypolias, P., 2015, Closure of the Paleotethys in the external Hellenides: Constraints from U–Pb ages of magmatic and detrital zircons (Crete): Gondwana Research, v. 28, p. 642–667.

Zulauf, G., Dörr, W., Krahl, J., Lahaye, Y., Chatzaras, V., and Xypolias, P., 2016, U–Pb zircon and biostratigraphic data of high-pressure/low-temperature metamorphic rocks of the Talea Ori: tracking the Paleotethys suture in central Crete, Greece: International Journal of Earth Sciences, v. 105, p. 1901–1922.

FIGURE CAPTIONS

Figure 1 (a) Simplified geotectonic map of the Eastern Mediterranean region (after Jacobshagen 1986; Okay and Tüysüz 1999; Okay *et al.* 2006). (b) Simplified geological map of the study area NW of Konya (modified after Özcan *et al.* 1990) with sample locations indicated with the pre-fix T14.

Figure 2 Correlation panel showing different stratigraphic schemes and nomenclatures of the Palaeozoic and Mesozoic units exposed in the Konya area. The colour code labels equivalent formations described by different authors. (a) Informal stratigraphy by Robertson and Ustaömer (2009b) on a local scale where the Eldeş and Ardıçlı formations are not exposed. (b) Tectonostratigraphic subdivision into a lower autochthonous and an upper allochthonous unit (Eren *et al.* 2004). (c) Continuous stratigraphic succession (Özcan *et al.* 1988, 1990). (d) Revised stratigraphic column for the Palaeozoic and Lower Mesozoic succession west of Ardıçlı village (this study). The Halıcı Group is subdivided into the mélange and 'flysch' units based on our field observations (see Section 4.1 for details). Biostratigraphic data from: [1]Eren 1993a, [2]Eren 1993b, [3]Eren 1996, [4]Göğer and Kıral 1969, [5]Göncüoğlu *et al.* 2000, [6]Göncüoğlu *et al.* 2007, [7]Karaman 1986, [8]Kurt 1994, [9]Özcan *et al.* 1988, [10]Özcan *et al.* 1990, [11]Wiesner 1968.

Figure 3 Field photographs from the Konya area. (a) Low-grade metamorphosed, fine-grained sediments of the mélange unit. (b) Well-bedded sandstones of the 'flysch' unit (at the location of sample T14-36). (c) Mudrock, locally with silt laminae from the 'flysch' unit. (d) Brecciated limestone of the Bozdağ Formation (west of Ardıçlı). (e) Outcrop showing massive limestones of the Bozdağ Formation, depositionally overlain by sedimentary rocks of the 'flysch' unit (Ardıçlı valley). (f) Refolded fold in sediments of the mélange unit at the contact with a limestone block of the Bozdağ Formation (south of Meydanlı). Dotted and solid white lines show relatively older and younger traces of axial surfaces. (g) View to the Southeast (Southeast of Ardıçlı Dam), the characteristic purple coloured sediments of the Triassic Ardıçlı Formation. (h) Massive, well-bedded Mesozoic limestone (partly dolomitic) (west of Ardıçlı). Hammer for scale in a–c, f, and h is about 30 cm long.

Figure 4 (a) Chemical classification scheme for siliciclastic sediments (after Herron, 1988) (b) QFL diagram for lithological classification of sandstones (after Dott, 1964). Sample T14-30 (conglomerate) is not shown.

Figure 5 Photomicrographs (cross-polarized light) of sediments from the Halıcı and Ardıçlı formations. (a) Strongly altered subarkose (mélange unit). (b) Mature quartz arenite ('flysch' unit). (c) Low-grade metamorphosed lithic wacke with mica beards (mélange unit). (d) Poorly sorted lithic wacke (block within mélange unit). (e) Initial sericitization of plagioclase ('flysch' unit). (f) Metaconglomerate with deformed sedimentary fragments (Ardıçlı Formation). (g, h) Sandstone samples from the Ardıçlı Formation.

Figure 6 Photomicrographs (cross-polarized light) showing the main types of lithic fragments in sediments from the study area. (a) Low-grade metasedimentary fragment (Lms: mica schist) in the mélange unit. (b) Large elongate (c. 4 mm) quartzitic fragment in the mélange unit. (c) Strongly altered sedimentary fragment (Ls) in the mélange unit. (d) Low-grade metasedimentary (Lms: mica-schist) fragment in the mélange unit. (e) Fine-grained sedimentary fragment in a block of the mélange unit. (f) Low-grade metasedimentary fragments (mica-schists) in the 'flysch' unit. (g) Chert fragment in the 'flysch' unit. (h) Volcanic fragment with plagioclase laths and needles in the Ardıçlı Formation. Abbreviations: L_s = sedimentary lithoclast; L_{ms} = metasedimentary lithoclast; L_m = metamorphic lithoclast; L_v = volcanic lithoclast.

Figure 7 Correlation diagrams of SiO_2, TiO_2, Na_2O, Fe_2O_3, CaO, K_2O and Rb versus Al_2O_3 and CaO versus LOI (loss on ignition). Data for UCC and PAAS from Rudnick and Gao (2003) and Taylor and McLennan (1985), respectively.

Figure 8 (a–c) UCC-normalized multi-element diagrams for samples from the Halıcı and Ardıçlı formations. Normalizing values from Rudnick and Gao (2003). (d–f) Chondrite-normalized REE diagrams for samples from the Halıcı and Ardıçlı formations. Normalizing values from Boynton (1984). Grey shaded areas indicate data from Triassic and Pennsylvanian–Cisuralian sediments from the Karaburun Peninsula (Löwen *et al*. 2018). Pm and Tm (bold) were not measured.

Figure 9 Discrimination diagrams for identifying (ultra)mafic provenance. (a) Ternary Ni–V–Th×10 plot for source rock discrimination after Bracciali *et al.* (2007) with source rock endmembers highlighted in grey. (b) Correlation diagram of Cr and Ni. High concentrations of Cr (>150 ppm) and Ni (>100 ppm) combined with Cr/Ni ratios ranging from 1.3 to 1.5 are indicative of an ultramafic provenance. (c) Cr/V versus Y/Ni diagram after McLennan *et al.* (1993). (Ultra)mafic sources are enriched in compatible elements (Cr, Ni) and tend towards high Cr/V and low Y/Ni ratios. (d) Th/Sc versus Cr/Th diagram. Felsic rocks are characterized by enrichment of incompatible elements (Th) and mafic sources have higher concentrations of compatible elements (Cr, Sc).

Figure 10 Histograms showing the age spectra for LA-ICP-MS zircon data of samples from the Halıcı and Ardıçlı formations. Sample T14-34 (e) represents a block within the mélange unit.

Figure 11 (a) Plot of Nb versus Cr contents of detrital rutiles for discrimination between

metamafic and metapelitic grains (linear slope after Triebold *et al.* 2012) (b) Histograms of calculated formation temperatures for analysed rutiles from the Halıcı and Ardıçlı formations. Number of measurements (n) in both types of diagrams varies depending on the number of grains with Nb, Cr or Zr below the detection limit.

Figure 12 Tectonic discrimination diagrams for samples from the Halıcı and Ardıçlı formations (this study). For comparison, data from a previous study of the Halıcı Formation (Kurt 1997) and from the Karaburun Peninsula (Löwen *et al.* 2018) are plotted as well. (a) K_2O/Na_2O versus SiO_2 diagram after Roser and Korsch (1986). PM – passive margin; ACM – active continental margin; ARC – oceanic island arc. (b) Multidimensional diagram after Verma and Armstrong-Altrin (2013). Discriminant functions (DF) based on major element oxides. Arc – island or continental arc; Rift – continental rift; Col – collision. (c and d) Multidimensional discriminant function diagrams based on major and selected trace elements after Verma and Armstrong-Altrin (2016). Discriminant functions were calculated using revised equations published in the corrigendum to Verma and Armstrong-Altrin (2016). In cases where samples show 0% concentrations of a specific element, the concentrations were set to 0.0001% in order to allow calculation of K_2O/Na_2O and $\log_e$-ratios for discriminant diagrams.

Figure 13 Diagram showing the difference between measured crystallization ages for detrital zircon grains and the depositional age of the sediment versus cumulative proportion of detrital zircon ages from samples of the Halıcı Formation (after Cawood *et al.* 2012).

Figure 14 Schematic reconstructions of the palaeomargins with Eurasian and Gondwanan affinities for the (a) Middle Carboniferous and (b) Late Triassic time as inferred from geochemical and geochronological data. The terms 'Eurasian affinity' and 'Gondwanan affinity' are defined in Section 5. The new data of this study show that previous palaeotectonic models presented in the literature have to be treated with caution as it is difficult to explain the provenance signals. Further work is required to develop a comprehensive revised palaeotectonic model.

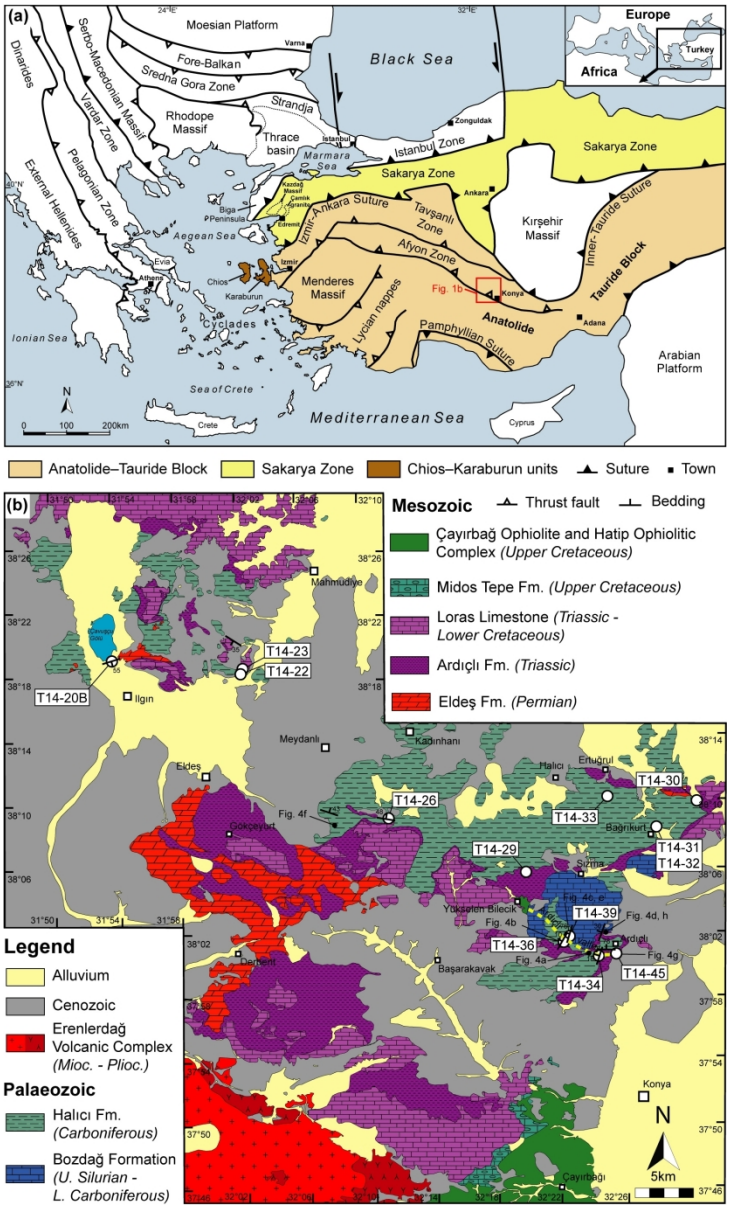

Figure 1: (a) Simplified geotectonic map of the Eastern Mediterranean region (after Jacobshagen 1986; Okay and Tüysüz 1999; Okay *et al.* 2006). (b) Simplified geological map of the study area NW of Konya (modified after Özcan *et al.* 1990) with sample locations indicated with the pre-fix T14.

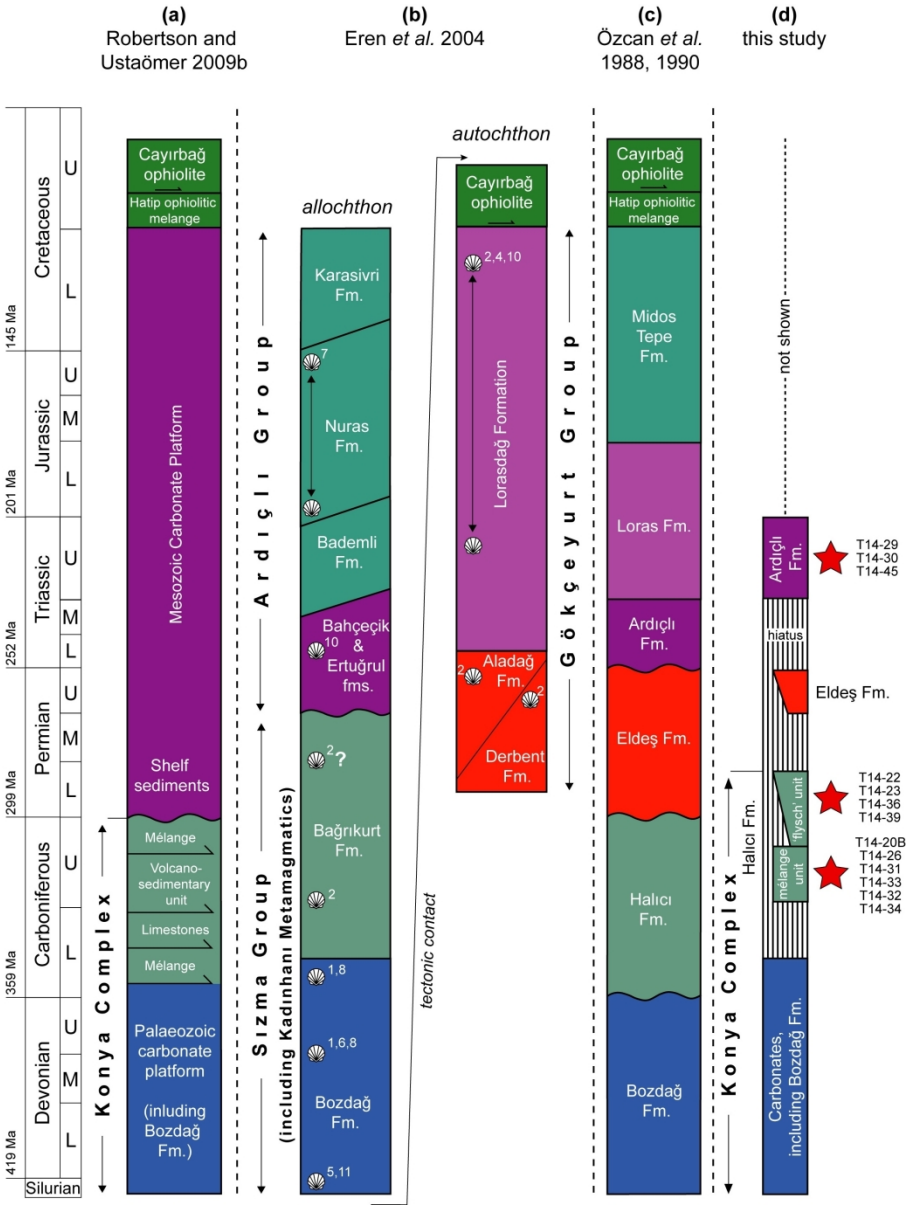

Figure 2: Correlation panel showing different stratigraphic schemes and nomenclatures of the Palaeozoic and Mesozoic units exposed in the Konya area. The colour code labels equivalent formations described by different authors. (a) Informal stratigraphy by Robertson and Ustaömer (2009b) on local scale where the Eldeş and Ardıçlı formations are not exposed. (b) Tectonostratigraphic subdivision into a lower autochthonous and an upper allochthonous unit (Eren *et al.* 2004). (c) Continuous stratigraphic succession (Özcan *et al.* 1988, 1990). (d) Revised stratigraphic column for the Palaeozoic and Lower Mesozoic succession west of Ardıçlı village (this study). The Halıcı Group is subdivided into the mélange and 'flysch' units based on our field observations (see Section 4.1 for details). Biostratigraphic data from: [1]Eren 1993a, [2]Eren 1993b, [3]Eren 1996, [4]Göğer and Kıral 1969, [5]Göncüoğlu *et al.* 2000, [6]Göncüoğlu *et al.* 2007, [7]Karaman 1986, [8]Kurt 1994, [9]Özcan *et al.* 1988, [10]Özcan *et al.* 1990, [11]Wiesner 1968.

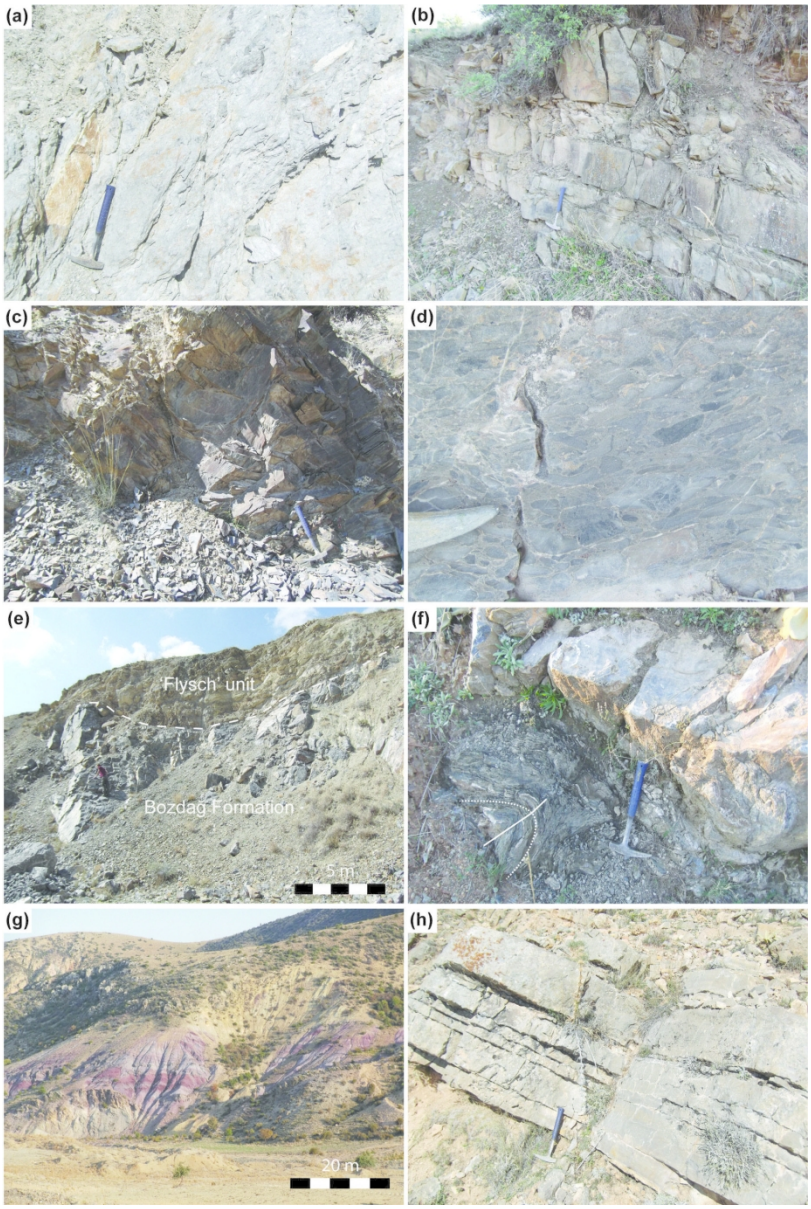

Figure 3: Field photographs from the Konya area. (a) Low-grade metamorphosed, fine-grained sediments of the mélange unit. (b) Well-bedded sandstones of the 'flysch' unit (at location of sample T14-36). (c) Mudrock, locally with silt laminae from the 'flysch' unit. (d) Brecciated limestone of the Bozdağ Formation (west of Ardıçlı). (e) Outcrop showing massive limestones of the Bozdağ Formation, depositionally overlain by sedimentary rocks of the 'flysch' unit (Ardıçlı valley). (f) Refolded fold in sediments of the mélange unit at the contact with a limestone block of the Bozdağ Formation (south of Meydanlı). Dotted and solid white lines show relatively older and younger traces of axial surfaces. (g) View to the Southeast (Southeast of Ardıçlı Dam), the characteristic purple coloured sediments of the Triassic Ardıçlı Formation. (h) Massive, well-bedded Mesozoic limestone (partly dolomitic) (west of Ardıçlı). Hammer for scale in a–c, f, and h is about 30 cm long.

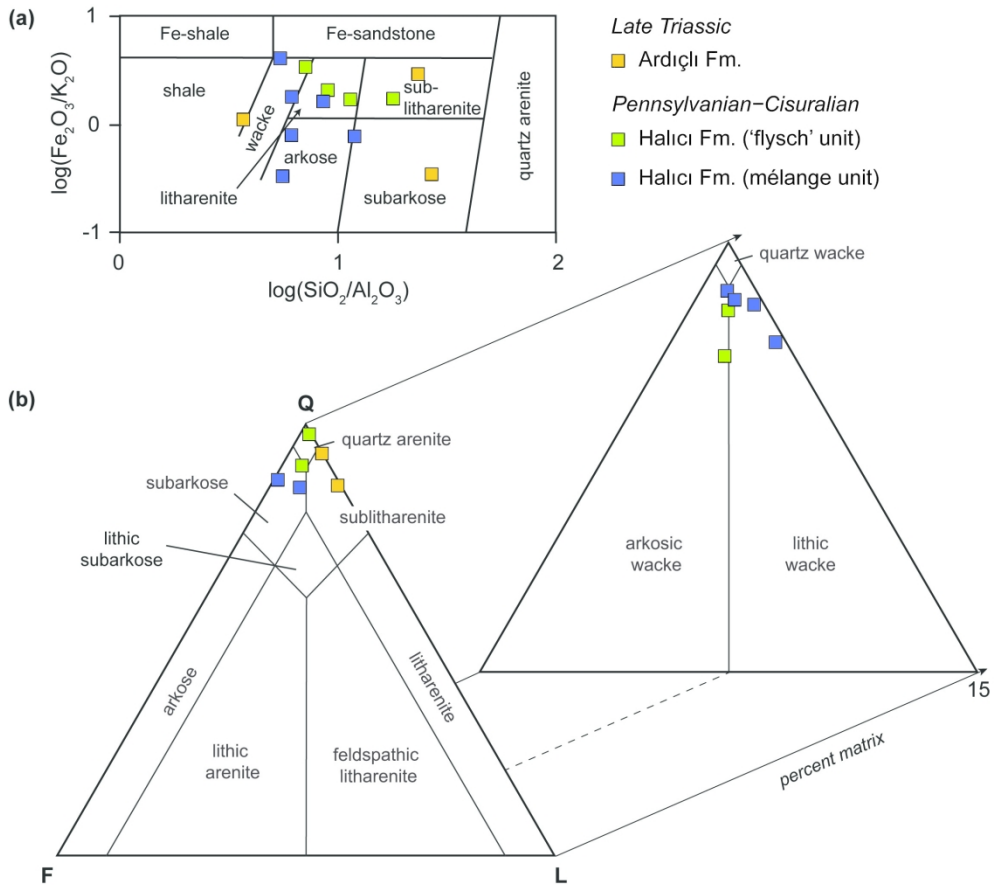

Figure 4: (a) Chemical classification scheme for siliciclastic sediments (after Herron, 1988) (b) QFL diagram for lithological classification of sandstones (after Dott, 1964). Sample T14-30 (conglomerate) is not shown.

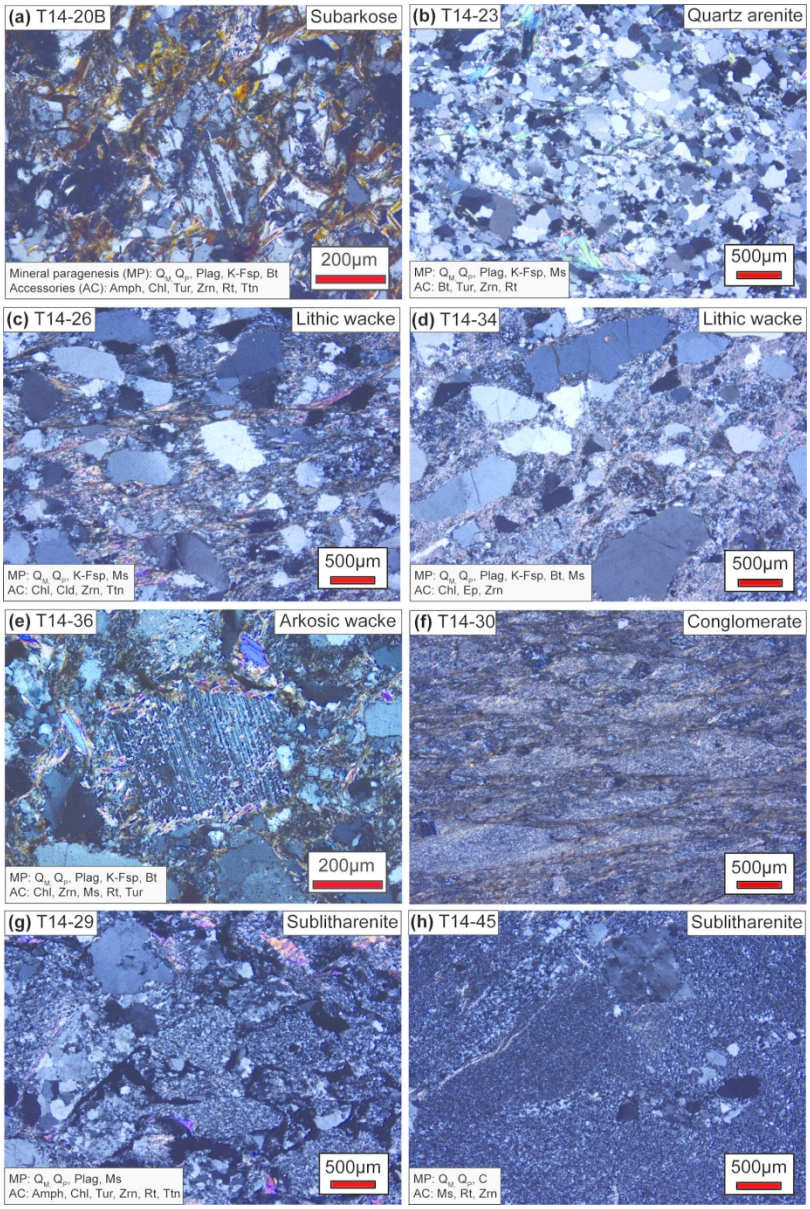

Figure 5: Photomicrographs (cross-polarized light) of sediments from the Halıcı and Ardıçlı formations. (a) Strongly altered subarkose (mélange unit). (b) Mature quartz arenite (‘flysch’ unit). (c) Low-grade metamorphosed lithic wacke with mica beards (mélange unit). (d) Poorly sorted lithic wacke (block within mélange unit). (e) Initial sericitisation of plagioclase (‘flysch’ unit). (f) Metaconglomerate with deformed sedimentary fragments (Ardıçlı Formation). (g, h) Sandstone samples from the Ardıçlı Formation.

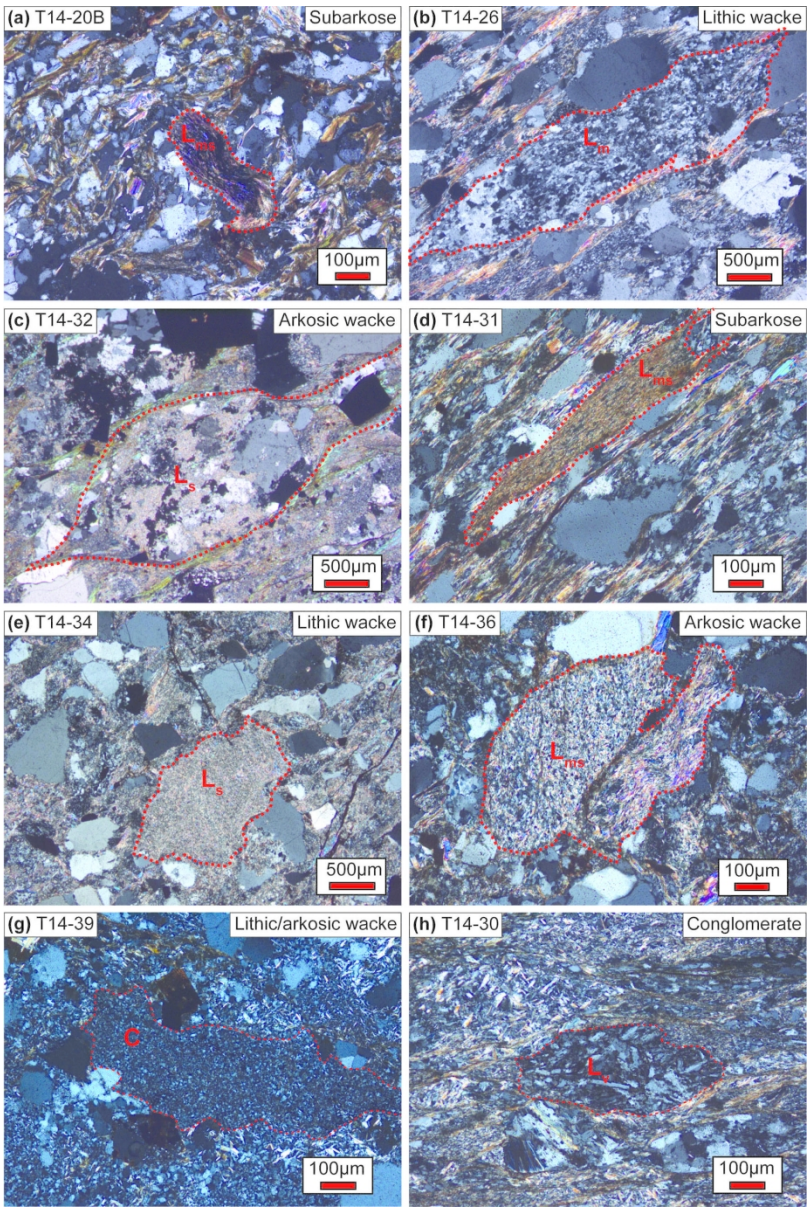

Figure 6: Photomicrographs (cross-polarized light) showing the main types of lithic fragments in sediments from the study area. (a) Low-grade metasedimentary fragment (L_{ms}: mica schist) in the mélange unit. (b) Large elongate (c. 4 mm) quartzitic fragment in the mélange unit. (c) Strongly altered sedimentary fragment (L_s) in the mélange unit. (d) Low-grade metasedimentary (L_{ms}: mica-schist) fragment in the mélange unit. (e) Fine-grained sedimentary fragment in a block of the mélange unit. (f) Low-grade metasedimentary fragments (mica-schists) in the 'flysch' unit. (g) Chert fragment in the 'flysch' unit. (h) Volcanic fragment with plagioclase laths and needles in the Ardıçlı Formation. Abbreviations: L_s = sedimentary lithoclast; L_{ms} = metasedimentary lithoclast; L_m = metamorphic lithoclast; L_v = volcanic lithoclast.

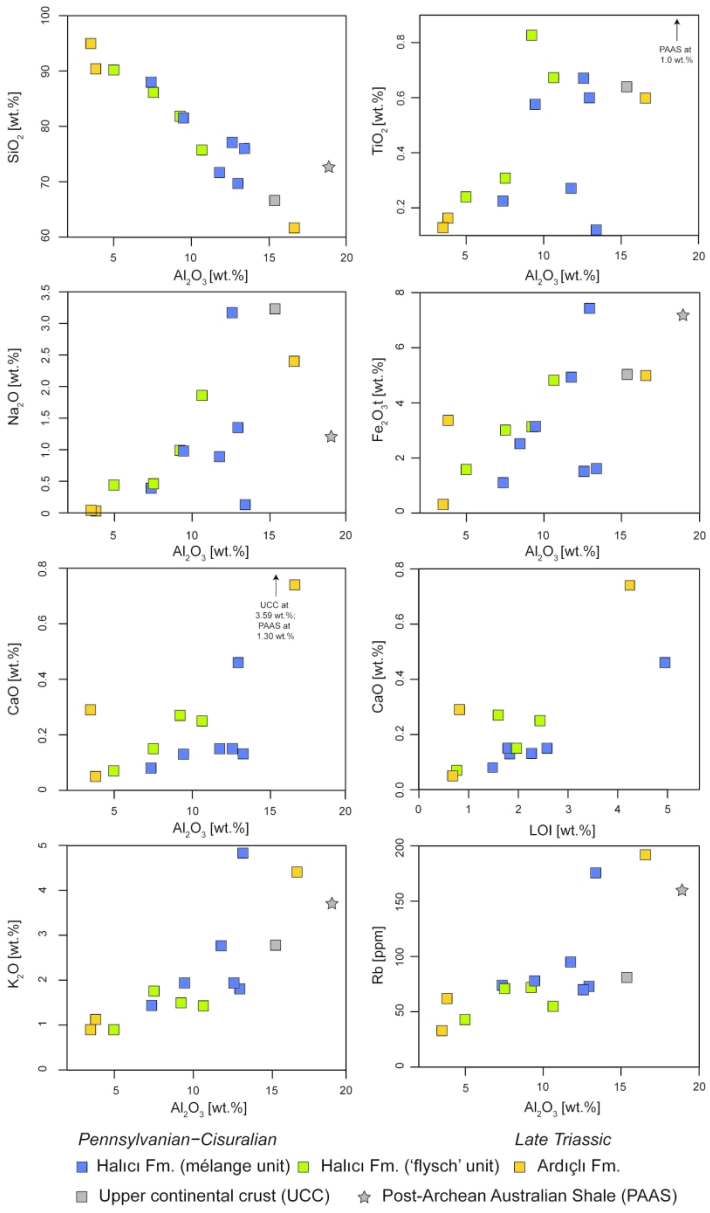

Figure 7: Correlation diagrams of SiO_2, TiO_2, Na_2O, Fe_2O_3, CaO, K_2O and Rb versus Al_2O_3 and CaO versus LOI (loss on ignition). Data for UCC and PAAS from Rudnick and Gao (2003) and Taylor and McLennan (1985), respectively.

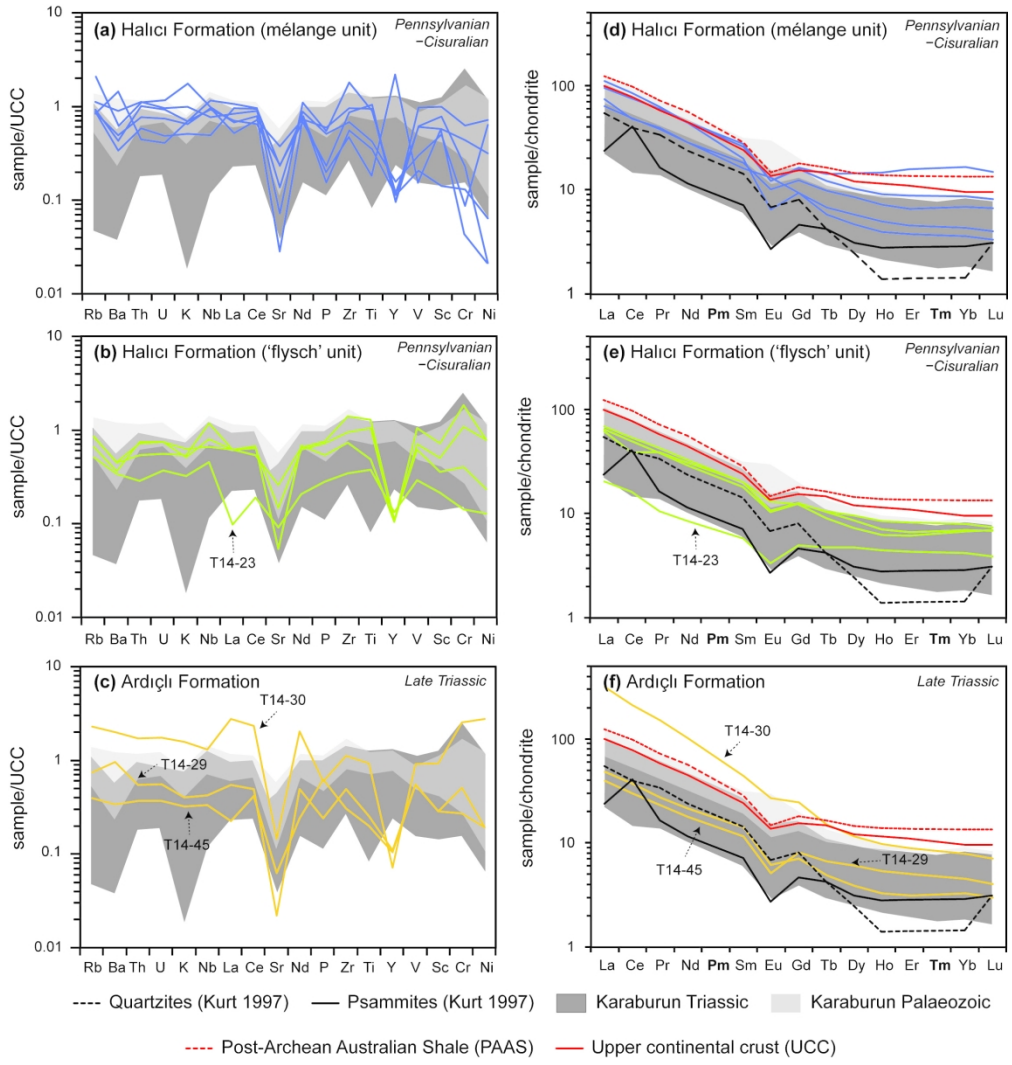

Figure 8: (a–c) UCC-normalized multielement diagrams for samples from the Halıcı and Ardıçlı formations. Normalizing values from Rudnick and Gao (2003). (d–f) Chondrite-normalized REE diagrams for samples from the Halıcı and Ardıçlı formations. Normalizing values from Boynton (1984). Grey shaded areas indicate data from Triassic and Pennsylvanian–Cisuralian sediments from the Karaburun Peninsula (Löwen *et al.* 2018). Pm and Tm (bold) were not measured.

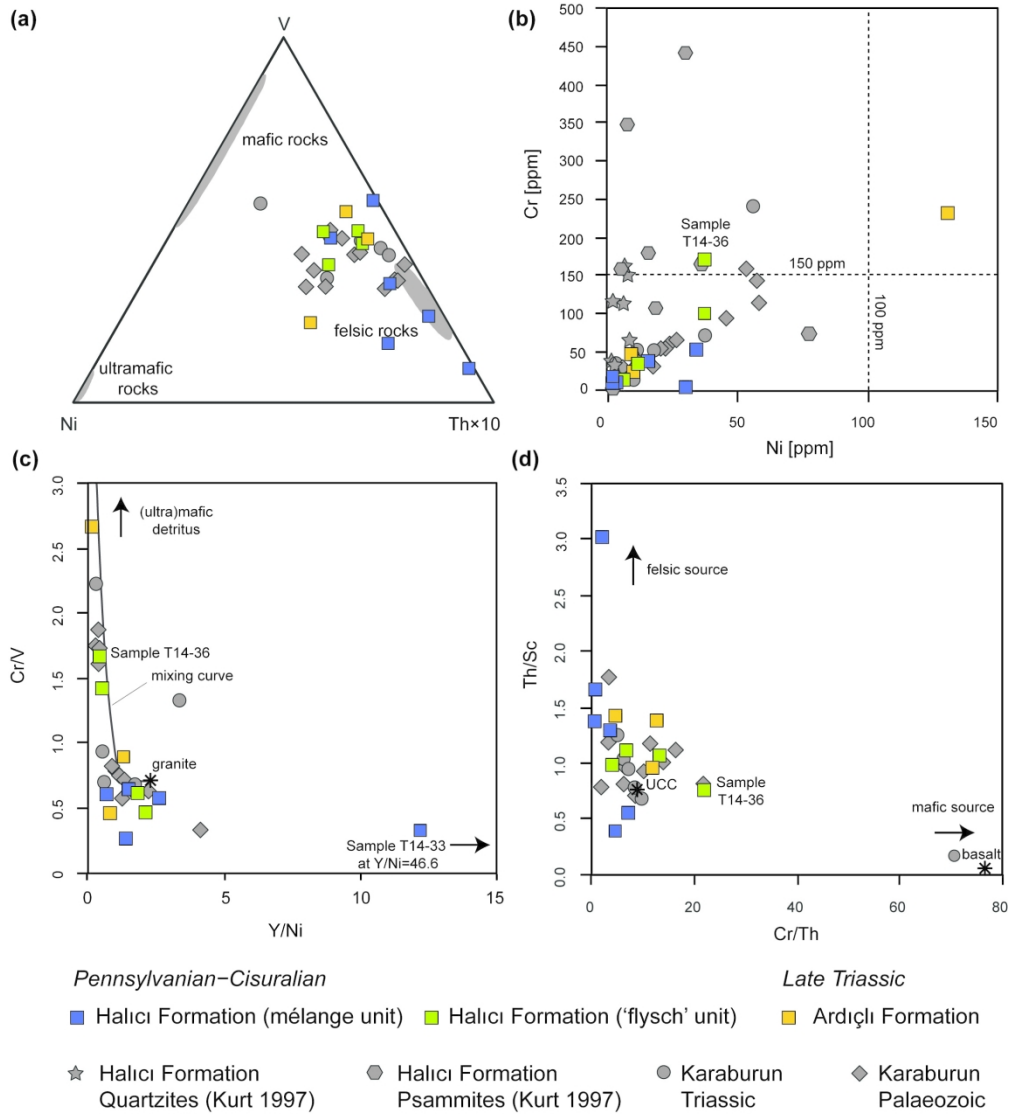

Figure 9: Discrimination diagrams for identifying (ultra)mafic provenance. (a) Ternary Ni–V–Th×10 plot for source rock discrimination after Bracciali *et al.* (2007) with source rock endmembers highlighted in grey. (b) Correlation diagram of Cr and Ni. High concentrations of Cr (>150 ppm) and Ni (>100 ppm) combined with Cr/Ni ratios ranging from 1.3 to 1.5 are indicative of an ultramafic provenance. (c) Cr/V versus Y/Ni diagram after McLennan *et al.* (1993). (Ultra)mafic sources are enriched in compatible elements (Cr, Ni) and tend towards high Cr/V and low Y/Ni ratios. (d) Th/Sc versus Cr/Th diagram. Felsic rocks are characterized by enrichment of incompatible elements (Th) and mafic sources have higher concentrations of compatible elements (Cr, Sc).

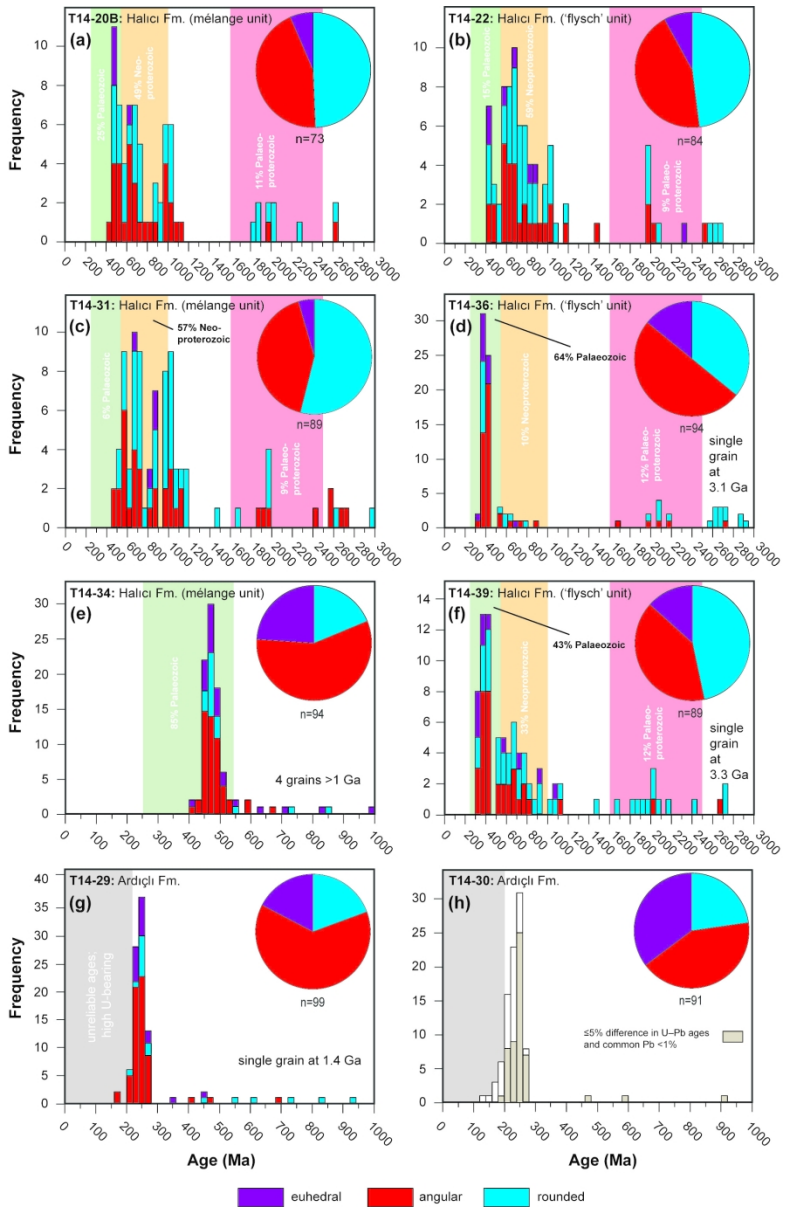

Figure 10: Histograms showing the age spectra for LA-ICP-MS zircon data of samples from the Halıcı and Ardıçlı formations. Sample T14-34 (e) represents a block within the mélange unit.

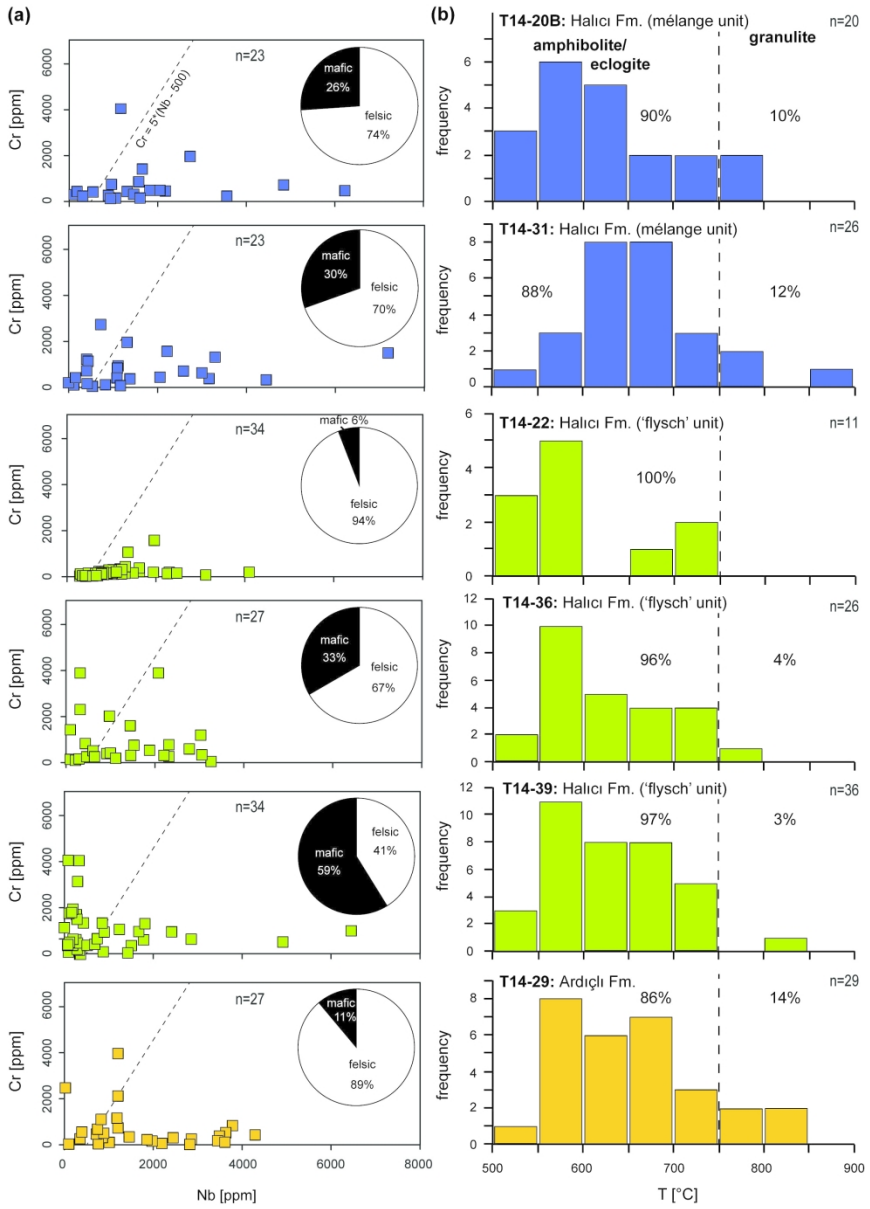

Figure 11: (a) Plot of Nb versus Cr contents of detrital rutiles for discrimination between metamafic and metapelitic grains (linear slope after Triebold *et al.* 2012) (b) Histograms of calculated formation temperatures for analyzed rutiles from the Halıcı and Ardıçlı formations. Number of measurements (n) in both types of diagrams varies depending on the number of grains with Nb, Cr or Zr below detection limit.

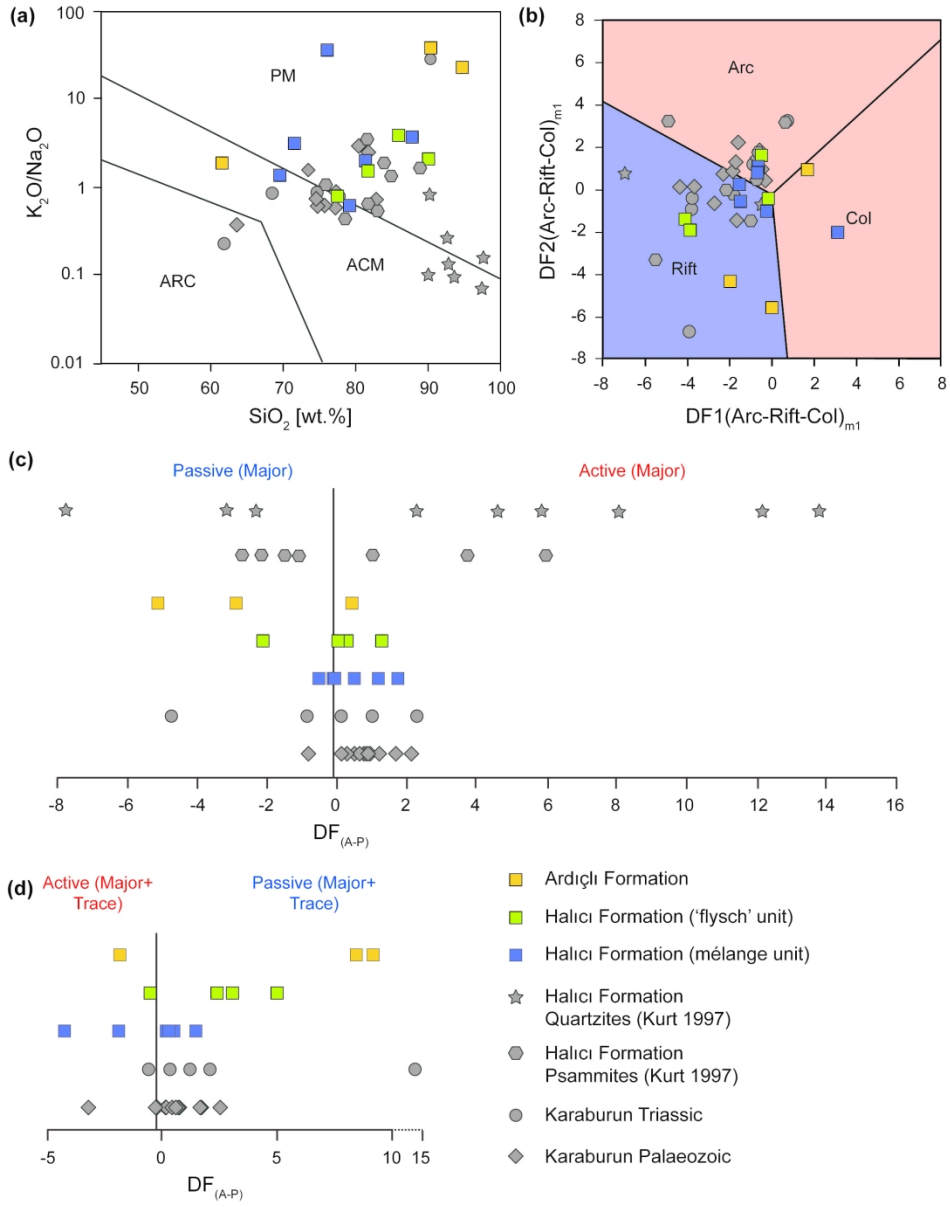

Figure 12: Tectonic discrimination diagrams for samples from the Halıcı and Ardıçlı formations (this study). For comparison, data from a previous study of the Halıcı Formation (Kurt 1997) and from the Karaburun Peninsula (Löwen *et al.* 2018) are plotted as well. (a) K_2O/Na_2O versus SiO_2 diagram after Roser and Korsch (1986). PM – passive margin; ACM – active continental margin; ARC – oceanic island arc. (b) Multidimensional diagram after Verma and Armstrong-Altrin (2013). Discriminant functions (DF) based on major element oxides. Arc – island or continental arc; Rift – continental rift; Col – collision. (c and d) Multidimensional discriminant function diagrams based on major and selected trace elements after Verma and Armstrong-Altrin (2016). Discriminant functions were calculated using revised equations published in the corrigendum to Verma and Armstrong-Altrin (2016). In cases where samples show 0% concentrations of a specific element, the concentrations were set to 0.0001% in order to allow calculation of K_2O/Na_2O and $\log_e$-ratios for discriminant diagrams.

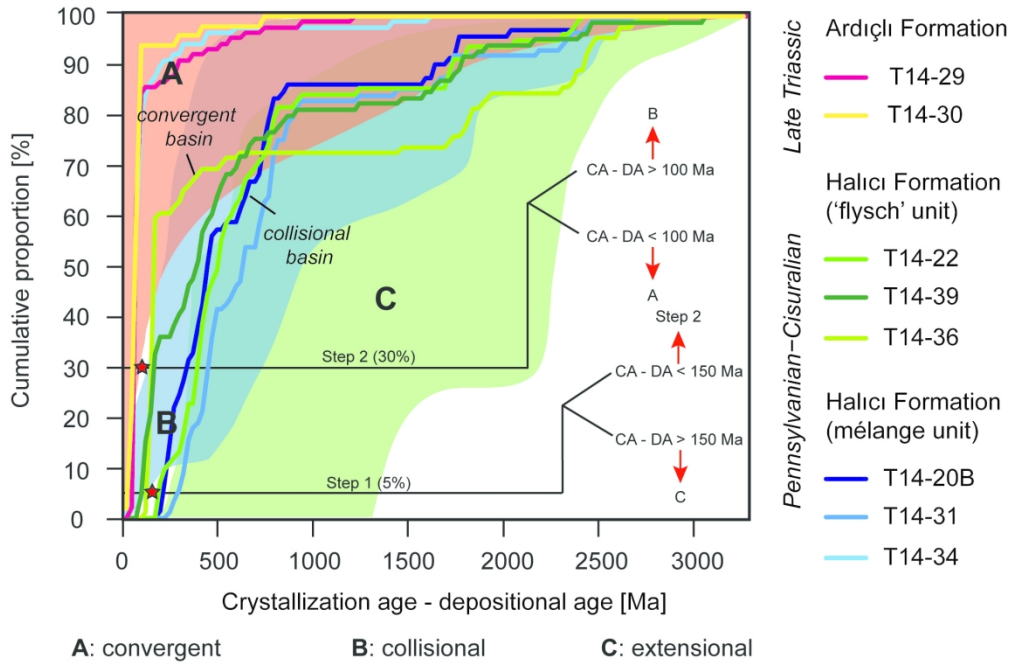

Figure 13: Diagram showing the difference between measured crystallization ages for detrital zircon grains and the depositional age of the sediment versus cumulative proportion of detrital zircon ages from samples of the Halıcı Formation (after Cawood *et al.* 2012).

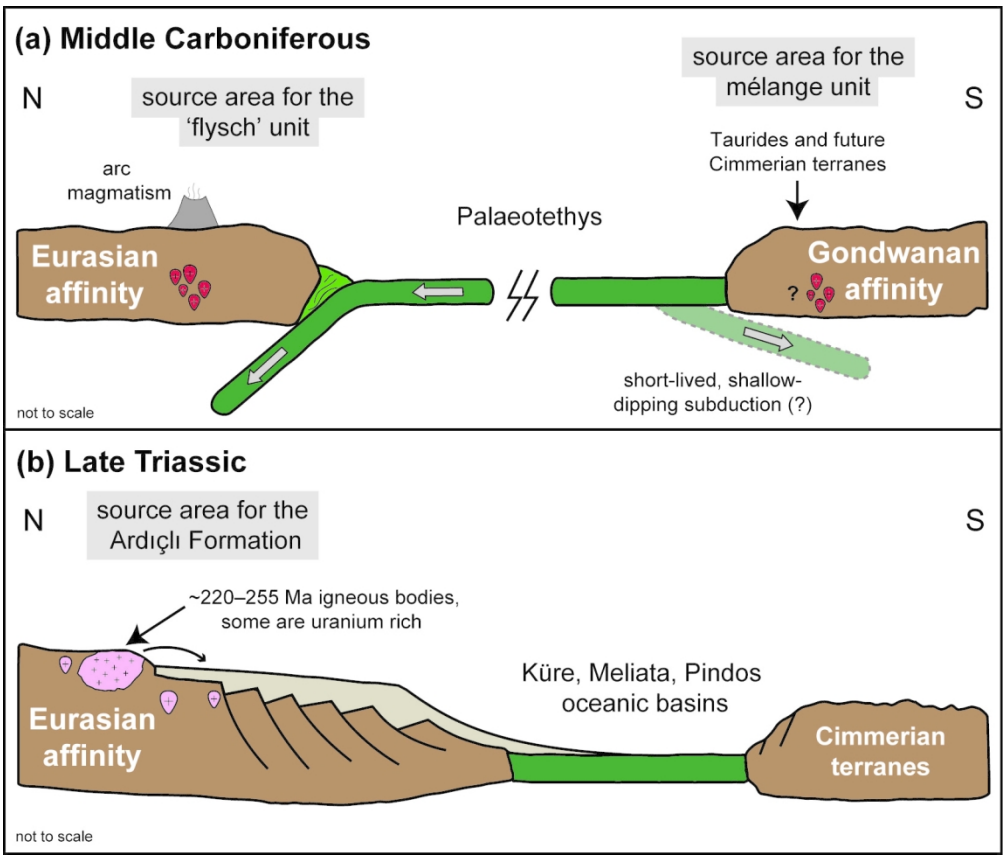

Figure 14: Schematic reconstructions of the palaeomargins with Eurasian and Gondwanan affinities for the (a) Middle Carboniferous and (b) Late Triassic time as inferred from geochemical and geochronological data. The terms 'Eurasian affinity' and 'Gondwanan affinity' are defined in Section 5. The new data of this study show that previous palaeotectonic models presented in the literature have to be treated with caution as it is difficult to explain the provenance signals. Further work is required to develop a comprehensive revised palaeotectonic model.